Chapter 5

Base isolation systems

5.1 *Introduction*

The term *isolation* refers to the degree of interaction between objects. An object is said to be isolated if it has little interaction with other objects. The act of *isolating* an object involves providing an interface between the object and its neighbors which minimizes interaction. These definitions apply directly to various physical systems. For example, one speaks of isolating a piece of equipment from its support by mounting the equipment on an isolation system which acts as a buffer between the equipment and the support. The design of isolation systems for vibrating machinery is a typical application. The objective here is to minimize the effect of the machine induced loading on the support. Another application is concerned with minimizing the effect of support motion on the structure. This issue is becoming increasingly more important for structures containing motion sensitive equipment and also for structures located adjacent to railroad tracks or other sources of ground disturbance.

Although isolation as a design strategy for mounting mechanical equipment has been employed for over seventy years, only recently has the concept been seriously considered for civil structures, such as buildings and bridges, subjected to ground motion. This type of excitation interacts with the structure at the foundation level, and is transmitted up through the structure. Therefore, it is logical to *isolate* the structure at its base, and prevent the ground

motion from acting on the structure. The idea of seismic isolation dates back to the late nineteenth century, but the application was delayed by the lack of suitable commercial isolation components. Substantial development has occurred since the mid 1980's (Naeim and Kelly, 1999), and base isolation for certain types of civil structures is now considered to be a highly viable design option by the seismic engineering community, particularly in Japan (Wada, 1998), for moderate to extreme seismic excitation.

A set of simple examples are presented in the next section to identify the key parameters and illustrate the quantitative aspects of base isolation. This material is followed by a discussion of practical aspects of seismic base isolation and a description of some seismically isolated buildings. The remaining sections deal with the behavioral and design issues for base isolated MDOF structural systems. Numerical results illustrating the level of performance feasible with seismic base isolation are included to provide a basis of comparison with the other *motion control* schemes considered in this text.

5.2 *Isolation for SDOF systems*

The application of base isolation to control the motion of a SDOF system subjected to ground motion was discussed earlier in Section 1.3 as part of a general treatment of design for dynamic excitation. The analytical formulation developed in that section provides the basis for designing an isolation system for simple structures that can be accurately represented with a SDOF model. Examples illustrating the reasoning process one follows are presented below. The formulation is also extended to deal with a modified version of a SDOF model that is appropriate for a low-rise building isolated at its base. This model is useful for preliminary design.

SDOF examples

The first example considers external periodic forcing of the SDOF system shown in Fig. 5.1. The solution of this problem is contained in Section 1.3. For convenience, the relevant equations are listed below:

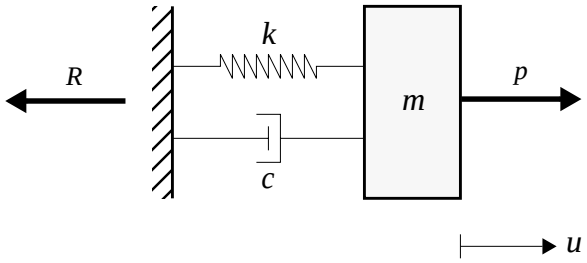

Fig. 5.1: SDOF system.

$$p = \hat{p}\sin\Omega t \tag{5.1}$$

$$u = \hat{u}\sin(\Omega t - \delta) \tag{5.2}$$

$$\hat{u} = \left[\frac{H_1}{k}\right]\hat{p} \tag{5.3}$$

$$H_1 = \frac{1}{\sqrt{[1-\rho^2]^2 + [2\xi\rho]^2}} \tag{5.4}$$

$$\rho = \frac{\Omega}{\omega} \tag{5.5}$$

$$\tan\delta = \frac{2\xi\rho}{1-\rho^2} \tag{5.6}$$

Given $\hat{p}$ and Ω, one can determine $\hat{u}$ for a specific system having mass m, stiffness k, and damping c. With $\hat{u}$ known, the forces in the spring and damper can be evaluated. The reaction can be found by either summing the internal forces, or combining p with the inertia force. With the latter approach, one writes

$$R = p - m\ddot{u} \tag{5.7}$$

and expands the various terms using eqns (5.1) through (5.6). The result is expressed as

$$R = \hat{R}\sin(\Omega t - \delta_r) \tag{5.8}$$

$$\hat{R} = H_3\hat{p} \tag{5.9}$$

$$H_3 = \sqrt{\frac{1 + [2\xi\rho]^2}{[1-\rho^2]^2 + [2\xi\rho]^2}} \tag{5.10}$$

$$\tan\delta_r = -\frac{\rho^2 H_1 \sin\delta}{1 + \rho^2 H_1 \cos\delta} \tag{5.11}$$

The function, H_3, is referred to as the transmissibility of the system. It is a measure of how much of the load p is transmitted to the support. When $\xi = 0$, $\delta = 0$ and H_3 reduces to H_1. Figure 5.2 shows the variation of H_3 with ρ and ξ.

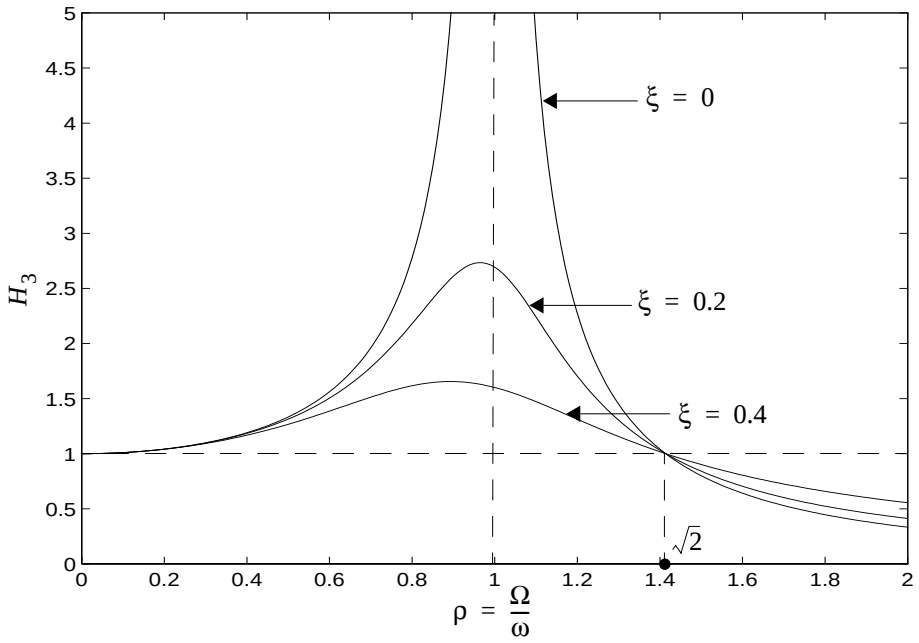

Fig. 5.2: Plot of H_3 versus ρ.

The model presented above can be applied to the problem of designing a support system for a machine with an eccentric rotating mass. Here, one wants to minimize the reaction force for a given $\hat{p}$, i.e. one takes $H_3 < 1$. Noting Fig. 5.2, this constraint requires the frequency ratio, ρ, to be greater than $\sqrt{2}$, and it follows that

$$\omega < \frac{\Omega}{\sqrt{2}} \tag{5.12}$$

The corresponding periods are related by

$$T > T_f\sqrt{2} = \sqrt{2}\left(\frac{2\pi}{\Omega}\right) \tag{5.13}$$

where T_f is the forcing period. For example, taking $T = 3T_f$ results in $\hat{R} = 0.125\hat{p}$, a reduction of 87.5% from the static value.

The second example illustrates the strategy for isolating a system from support motion. Applying the formulation derived in Section 1.4 to the system shown in Fig. 5.3, the amplitudes of the relative and total displacement of the mass, $\hat{u}$ and $\hat{u}_t$, are related to the support displacement by

$$\hat{u} = \rho^2 H_1 \hat{u}_g = H_2 \hat{u}_g \tag{5.14}$$

$$\hat{u}_t = H_3 \hat{u}_g \tag{5.15}$$

Taking H_3 small with respect to unity reduces the effect of support motion on the position of the mass. The frequency and period criteria are the same as those of the previous example. One takes $\rho > \sqrt{2}$ to reduce $\hat{u}_t$. However, since H_2 approaches unity as ρ increases, the magnitude of the relative motion increases and approaches the ground motion, $\hat{u}_g$. Therefore, this relative motion needs to be accomodated.

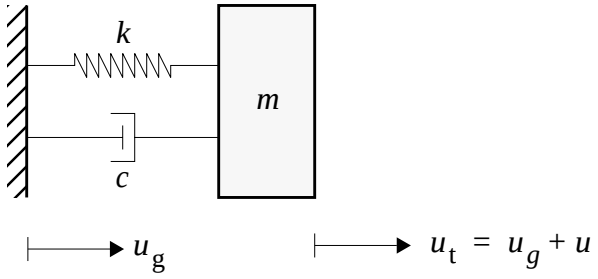

Fig. 5.3: SDOF system subjected to support motion.

These examples show that isolation is obtained by taking the period of the SDOF system to be large in comparison to the forcing (either external or support)

period. Expressing this requirement as

$$T \geq \rho^* T_f \qquad \Rightarrow \qquad \omega < \frac{\Omega}{\rho^*} \tag{5.16}$$

where ρ^* depends on the desired reduction in amplitude, the constraint on the stiffness of the spring is given by

$$k < m\left[\frac{\Omega}{\rho^*}\right]^2 = m\left[\frac{2\pi}{\rho^* T_f}\right]^2 \tag{5.17}$$

It should be noted that this derivation assumes that a single periodic excitation is applied. The result is applicable for ***narrow band*** excitations which are characterized by a dominant frequency. A more complex analysis involving iteration on the stiffness is required to deal with ***broad band*** excitations. One has to ensure that the forcing near the fundamental frequency is adequately controlled by damping in this case.

Bearing terminology

The spring and damper elements connecting the mass to the support are idealizations of physical objects called *bearings*. They provide a constraint against motion relative to a support plane, as illustrated in Fig. 5.4. The bearing in Fig. 5.4(a) functions as an axial element and resists the displacement normal to the plane with normal stresses (tension and compression). The bearing shown in Fig. 5.4(b) constrains relative tangential motion through shearing action over the height of the bearing. These elements are usually combined into a single compound bearing, but it is more convenient to view them as being uncoupled when modeling the system.

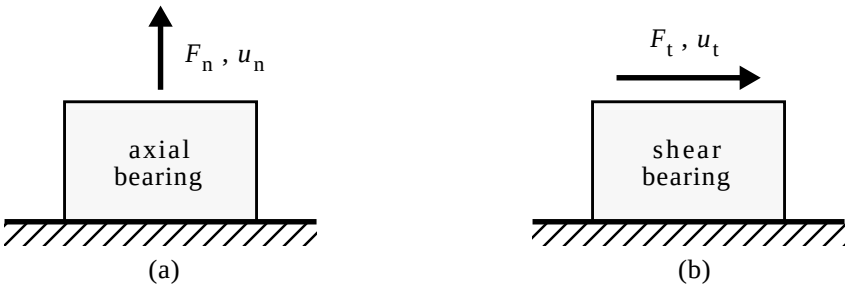

Fig. 5.4: Axial and shear bearings.

When applying the formulation developed above, one distinguishes between normal and tangential support motion. For *normal* motion, axial type bearings such as springs and rubber cushions are used; the k defined by eqn (5.17) is the axial stiffness of the bearing F_n / u_n. Shear bearings such as laminated rubber cushions and inverted pendulum type sliding devices are used when the induced motion is parallel to the ground surface. In this case, k represents the required *shearing* stiffness of the bearing, F_t / u_t.

Figure 5.5 shows an air spring/damper scheme used for vertical support. Single and multiple stage laminated rubber bearings are illustrated in Fig 5.6. Rubber bearings used for seismic isolation can range up to 1 m in diameter and are usually inserted between the foundation footings and the base of the structure. A particular installation for a building is shown in Fig 5.7.

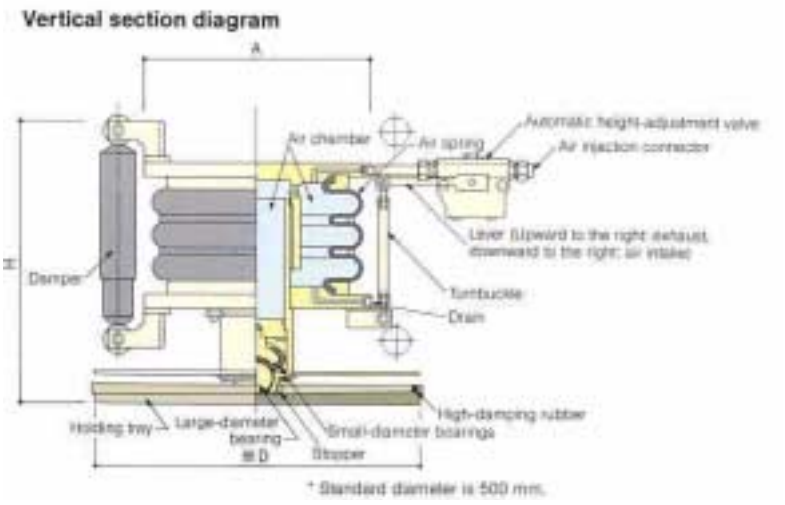

Fig. 5.5: Air spring bearing.

a) Single stage

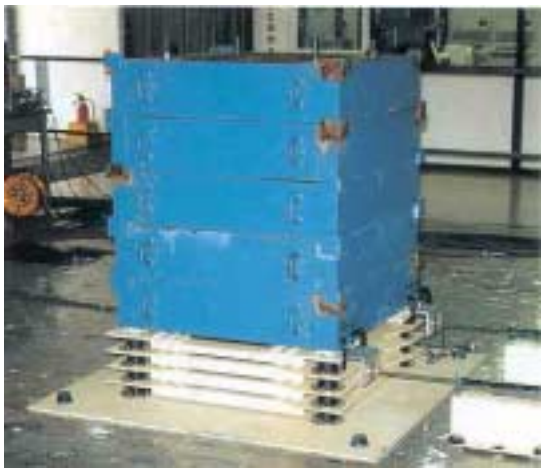

b) multiple stage

Fig. 5.6: Laminated rubber bearings.

Fig. 5.7: Rubber bearing seismic isolation system.

Modified SDOF Model

In what follows, the support motion is considered to be due to seismic excitation. Although both normal (vertical) and tangential (horizontal) motions occur during a seismic event, the horizontal ground motion is generally more significant for structural systems since it leads to lateral loading. Typical structural systems are designed for vertical loading and then modified for lateral loading. Since the vertical motion is equivalent to additional vertical loading, it is not as critical as the horizontal motion.

The model shown in Fig. 5.3 represents a rigid structure supported on flexible shear bearings. To allow for the flexibility of the structure, the structure can be modeled as a MDOF system. Figure 5.8 illustrates a SDOF beam type idealization. One can estimate the equivalent SDOF properties of the structure by assuming that the structural response is dominated by the fundamental mode. The data provided in earlier chapters shows that this assumption is reasonable for low-rise buildings subjected to seismic excitation.

An in-depth analysis of low rise buildings modeled as MDOF beams is presented later in this chapter. The objective here is to derive a simple relationship showing the effect of the bearing stiffness on the relative displacement of the

structure, u, with respect to the base displacement, $u_b + u_g$. The governing equations for the lumped mass model consist of an equilibrium equation for the mass, and an equation relating the shear forces in the spring and the bearing.

$$m\ddot{u} + c\dot{u} + ku = -m(\ddot{u}_b + \ddot{u}_g) \tag{5.18}$$

$$k_b u_b + c_b \dot{u}_b = ku + c\dot{u} \tag{5.19}$$

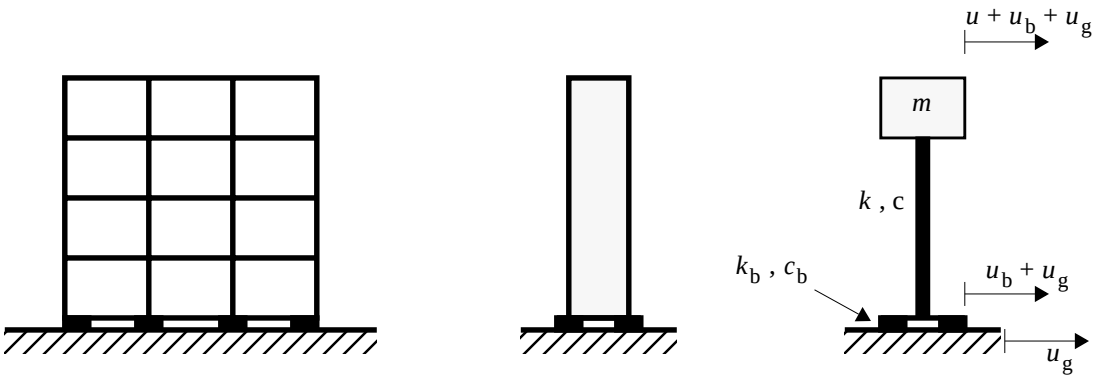

(a) Actual structure (b) Beam idealization (c) Lumped mass model

Fig. 5.8: Base isolation models.

Neglecting damping, eqn (5.19) can be solved for u_b in terms of u.

$$u_b = \left[\frac{k}{k_b}\right] u \tag{5.20}$$

Then, substituting for u_b in eqn (5.18) leads to

$$m\left[1 + \frac{k}{k_b}\right]\ddot{u} + ku = -m\ddot{u}_g \tag{5.21}$$

Equation (5.21) is written in the conventional form for a SDOF system

$$\ddot{u} + \omega_{eq}^2 u = -\Gamma \ddot{u}_g \tag{5.22}$$

where Γ is a participation factor,

$$\Gamma = \frac{k_b}{k + k_b} = \left(\frac{k_b}{k}\right) \Big/ \left(1 + \frac{k_b}{k}\right) \tag{5.23}$$

and ω_{eq} is an equivalent frequency measure

$$\omega_{eq}^2 = \frac{\Gamma k}{m} = \Gamma\omega^2 \tag{5.24}$$

In this case, ω_{eq} is the fundamental frequency of the system consisting of the structure plus bearing. Taking k_b small with respect to k decreases the inertia loading on the structure as well as the effective frequency. Consequently, the structural response is reduced.

Periodic excitation - modified SDOF model

To illustrate the effect of base stiffness on the response, the case of periodic ground motion, $u_g = \hat{u}_g \sin\Omega t$, is considered. The various response amplitudes are given by

$$\hat{u} = \frac{\Gamma\rho_{eq}^2}{\left|1-\rho_{eq}^2\right|}\hat{u}_g \tag{5.25}$$

$$\hat{u}_b = \left[\frac{k}{k_b}\right]\hat{u} \tag{5.26}$$

$$\hat{u}_t = \hat{u} + \hat{u}_b + \hat{u}_g = \frac{1}{\left|1-\rho_{eq}^2\right|}\hat{u}_g \tag{5.27}$$

where the brackets indicate absolute values, and ρ_{eq} is the frequency ratio

$$\rho_{eq} = \frac{\Omega}{\omega_{eq}} \tag{5.28}$$

Comparing eqn (5.27) with eqn (5.15) shows that the results are similar. One replaces ω with ω_{eq} in the expression for H_3. The limiting cases are $k_b = 0$ and $k_b = \infty$. The former is the fully isolated case where $u_b \approx -\hat{u}_g$ and $u_t \approx 0$; the latter corresponds to a fixed support where $u_b \approx 0$ and $u_t \approx u + u_g$.

Suppose the structure is defined, and the problem concerns selecting a bearing stiffness such that the total response satisfies

$$\hat{u}_t \le \nu\hat{u}_g \qquad \nu < 1$$

One needs to take $\rho_{eq} > \sqrt{2}$. Noting eqn (5.27), the required value of ρ_{eq} is

$$\rho_{eq}^2 = 1 + \frac{1}{\nu} \tag{5.29}$$

Substituting for ρ_{eq} in eqn (5.28) leads to

$$\omega_{eq}^2 = \frac{\Omega^2}{1 + \frac{1}{\nu}} \tag{5.30}$$

Finally, using eqn (5.23) and (5.24), the required bearing stiffness is given by

$$k_b = k\frac{1}{\left(\frac{k}{\omega_{eq}^2 m}\right) - 1} = \frac{k}{\frac{k(1 + (1/\nu))}{m\Omega^2} - 1} \tag{5.31}$$

The more general problem is the case where both structural stiffness and the bearing stiffness need to be established subject to the following constraints on the magnitudes of $\hat{u}$ and $\hat{u}_b$.

$$\begin{aligned} \hat{u} &= \nu_s \hat{u}_g \\ \hat{u}_b &= \nu_b \hat{u}_g \end{aligned} \tag{5.32}$$

The typical design scenario has ν_b larger than ν_s. Noting eqn (5.26), the stiffness factors are related by

$$k_b = \frac{\nu_s}{\nu_b} k \tag{5.33}$$

Equation (5.25) provides the second equation relating the stiffness factors. It reduces to

$$\left| -1 + \frac{1}{\rho_{eq}^2} \right| = \frac{\Gamma}{\nu_s} \tag{5.34}$$

where

$$\Gamma = \frac{k_b/k}{1 + k_b/k} = \frac{\nu_s}{\nu_s + \nu_b} \tag{5.35}$$

Solving eqn (5.34) for ρ_{eq}^2 leads to ω_{eq}^2 , and then k.

$$\omega_{eq}^2 = \frac{\Omega^2}{\rho_{eq}^2} = \Gamma \frac{k}{m} \tag{5.36}$$

The following example illustrates the computational steps.

Example 5.1: ***Stiffness factors for prescribed structure and base motion.***

Suppose $\nu_s = 0.1$ and $\nu_b = 1.0$. The relative motion of the base with respect to the ground is allowed to be 10 times greater than the relative motion of the structure with respect to the base.

$$\hat{u}_b = 10\hat{u} \tag{1}$$

The stiffness factors are related by

$$k_b = \frac{\nu_s}{\nu_b} k = 0.1k \tag{2}$$

Evaluating Γ and ρ_{eq} , using eqns (5.34) and (5.35),

$$\frac{\nu_s}{\nu_s + \nu_b} = \frac{0.1}{1.1} = 0.0909 \tag{3}$$

$$\left|1 - \frac{1}{\rho_{eq}^2}\right| = \frac{\Gamma}{\nu_s} = \frac{1}{1.1} = 0.909 \tag{4}$$

$$\rho_{eq}^2 = 11.0011$$

leads to

$$\omega_{eq}^2 = 0.0909\Omega^2 \tag{5}$$

and finally to k

$$k = \frac{m}{\Gamma}\omega_{eq}^2 = m\Omega^2 \tag{6}$$

Seismic excitation - modified SDOF model

An estimate of the stiffness parameters required to satisfy the motion constraints under seismic excitation can be obtained with the response spectra approach described in Chapter 2. Taking $\ddot{u}_g$ to be the seismic excitation, the solution of eqn (5.22) is related to the spectral velocity by

$$|u|_{max} = \frac{\Gamma S_v}{\omega_{eq}} \tag{5.37}$$

where S_v is a function of the equivalent frequency, ω_{eq}, and the equivalent damping ratio for the structure/bearing system, ξ_{eq}. Substituting for Γ and ω_{eq}, eqn (5.37) expands to

$$|u|_{max} = S_v\sqrt{\frac{mk_b}{k(k+k_b)}} \tag{5.38}$$

The relation between the maximum relative displacement of the bearing and the maximum structural motion follows from eqn (5.20)

$$|u_b|_{max} = \left[\frac{k}{k_b}\right]|u|_{max} \tag{5.39}$$

In this development, the criteria for motion based design of a base isolated structure are expressed as limits on the relative motion terms

$$|u|_{max} = u^* \tag{5.40}$$

$$|u_b|_{max} = u_b^* \tag{5.41}$$

The values of k and k_b required to satisfy these constraints follow by solving eqns (5.38) and (5.39).

$$k_b = \frac{ku^*}{u_b^*} \tag{5.42}$$

$$k = \frac{mS_v^2}{[u^*]^2}\left[\frac{1}{1+\dfrac{u_b^*}{u^*}}\right] = \frac{mS_v^2}{u^*(u^*+u_b^*)} \tag{5.43}$$

One assumes S_v is constant, evaluates k and k_b, determines the frequency ω_{eq} with eqn (5.24), and then updates S_v if necessary.

It is of interest to compare the stiffness required by the base isolated structure with the stiffness of the corresponding fixed base structure. Taking $k_b = \infty$ reduces eqn (5.38) to

$$|u|_{max} = S_v\sqrt{\frac{m}{k}} \tag{5.44}$$

The fixed base structural stiffness k_f follows from eqn (5.44)

$$k_f = |k|_{k_b=\infty} = \frac{mS_v^2}{[u^*]^2} \tag{5.45}$$

Using eqn (5.45) and assuming the value of S_v is the same for both cases, the stiffness ratios reduce to,

$$\frac{k}{k_f} = \left[\frac{1}{1+\dfrac{u_b^*}{u^*}}\right] \tag{5.46}$$

$$\frac{k_b}{k_f} = \left[\frac{\dfrac{u^*}{u_{b^*}}}{1+\dfrac{u_b^*}{u^*}}\right] \tag{5.47}$$

The ratio of the isolated period to the fixed base period can be generated with eqn (5.24)

$$\frac{T_{\text{eq}}}{T_f} = \frac{\omega_f}{\omega_{\text{eq}}} = 1 + \frac{u_{\text{b}}^*}{u^*} \tag{5.48}$$

Figures 5.9 and 5.10 show the variation of k/k_f and k_{b}/k_f with u_{b}^*/u^* for a given constant S_v. The increase in the period is plotted in Fig. 5.11. There is a significant reduction in the structural stiffness required by the seismic excitation when the base is allowed to move. For example, taking $u_{\text{b}}^* = 2u^*$ decreases the design stiffness by a factor of 3. However, one has to ensure that a potential resonant condition is not created by shifting the period. There may be a problem with wind gust loading as the period is increased beyond 3 seconds. This problem can be avoided by providing additional stiffness that functions under wind loading but not under seismic loading. Section 5.3 deals with this problem.

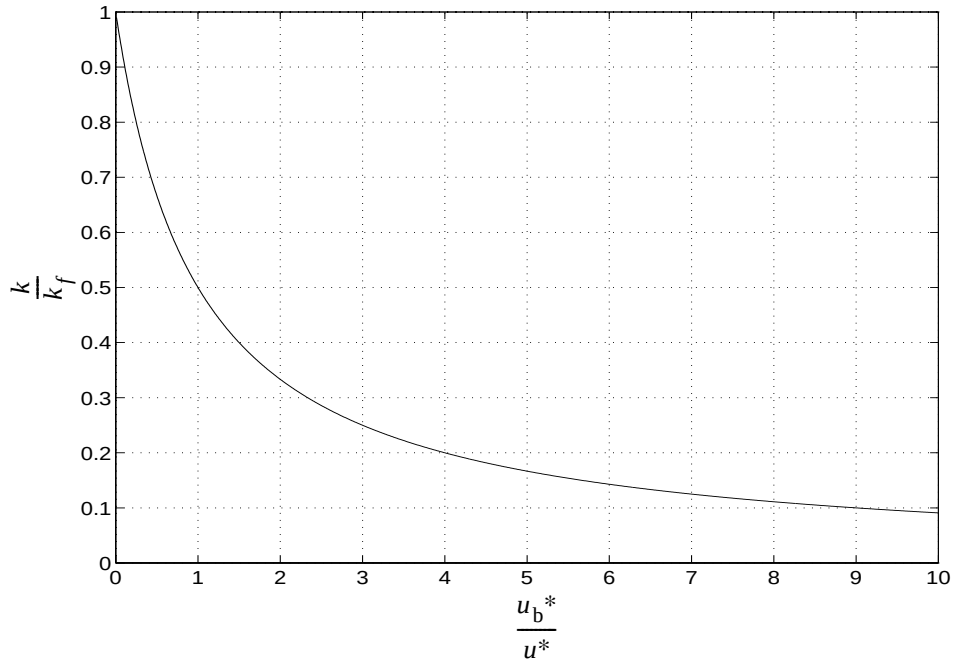

Fig. 5.9: Variation of k/k_f with u_{b}^*/u^*.

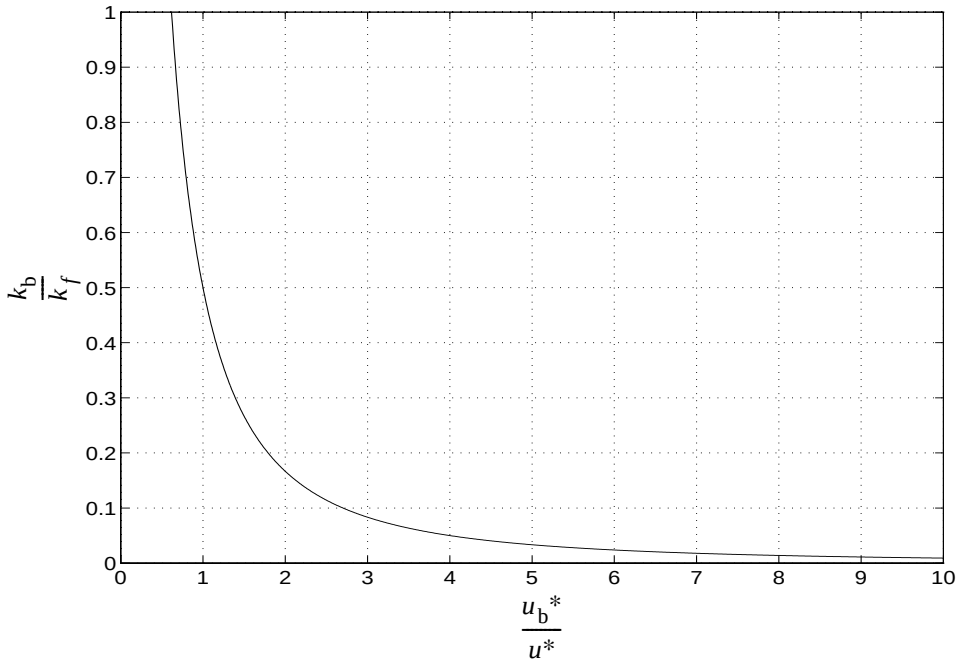

Fig. 5.10: Variation of k_b/k_f with u_b^*/u^*.

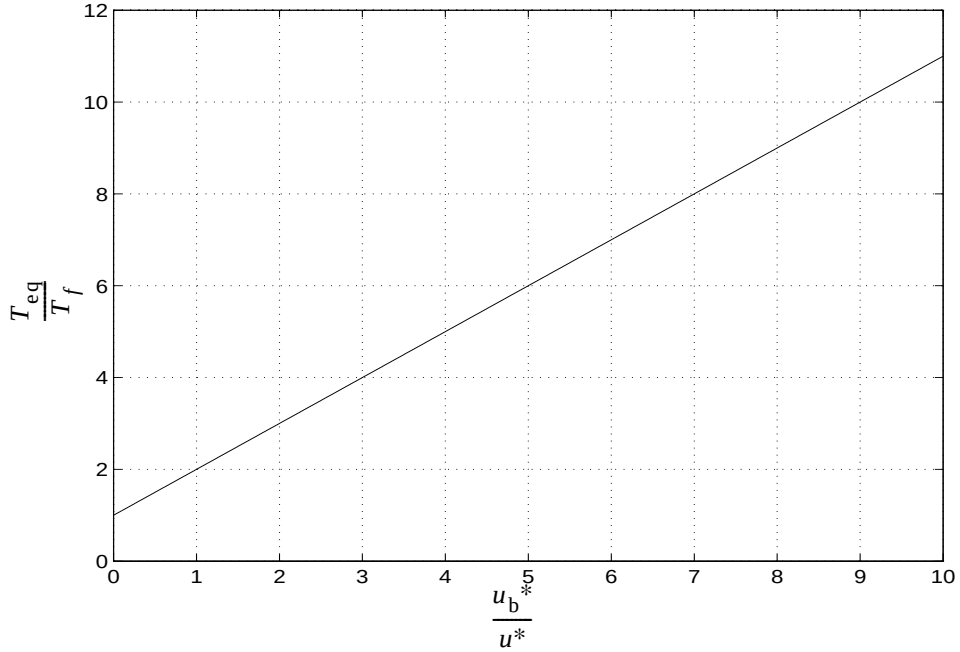

Fig. 5.11: Variation of T_{eq}/T_f with u_b^*/u^*.

Example 5.2:*Stiffness parameters - modified SDOF model of Building example #2.*

The procedure for establishing the appropriate values for u^* and $u_b{}^*$ is illustrated using building Example 2 as the reference structure. Table 2.4 lists the relevant design information. The period for the fixed base case is 1.06 sec. Since bad isolation increases the period, the assumption that S_v is constant is valid.

The relative displacement at the top of the building is estimated as $H\gamma^*$ where H is the height of the structure and γ^* is the prescribed shear deformation. Taking $H = 50\text{m}$ and $\gamma^* = 1/200$ leads to $u^* = 0.25\text{m}$.

The allowable bearing displacement depends on the bearing configuration and response characteristics, as well as the seismic excitation. For the totally *soft* case, u_b is equal to the ground excitation. Hardening the bearing reduces u_b somewhat, so a reasonable upper limit is the peak ground displacement corresponding to the design value of S_v for representative earthquakes. A typical design value for $u_b{}^*$ is 0.3m. Using $u^* = 0.25\text{m}$ and $u_b{}^* = 0.3\text{m}$ corresponds to the following stiffness factors

$$k = 0.455k_f$$

$$k_b = 0.833k$$

$$T = 2.2T_f$$

The required structural stiffness is reduced by 55% for this degree of base isolation.

These scenarios provide an indication of the potential benefit of base isolation for seismic excitation. However, one should note that the isolated structure is less stiff than the fixed base structure, and therefore will experience larger displacement under other types of loading such as wind. Also, the simplified model considered here is based on linear undamped behavior, whereas the actual bearings have some damping and may behave in a nonlinear manner. More complex models are considered in a later section.

5.3 *Design issues for structural isolation systems*

The most important requirements for an isolation system concern flexibility, energy dissipation, and rigidity under low level loading. A number of solutions have been proposed for civil type structures over the past thirty years. The most significant aspects of these designs is discussed below.

Flexibility

A structural isolation system generally consists of a set of flexible support elements that are proportioned such that the period of vibration of the isolated structure is considerably greater than the dominant period of the excitation. Systems proposed to date employ plates sliding on a curved surface (eg., an inverted pendulum), sleeved piles, and various types of rubber bearings. The most popular choice at this point in time is the rubber bearing, with about 90% of the applications.

Rubber bearings consist of layers of natural rubber sheets bonded to steel plates, as shown in Fig. 5.12. The steel plates constrain the lateral deformation of the rubber under vertical loading, resulting in a vertical stiffness several orders of magnitude greater than the horizontal stiffness. The lateral stiffness depends on the number and thickness of the rubber sheets. Increasing either quantity decreases the stiffness; usually one works with a constant sheet thickness and increases the number of layers. As the height increases, buckling becomes the controlling failure mechanism, and therefore, the height is usually limited to about half the diameter. Natural rubber is a nonlinear viscoelastic material, and is capable of deforming up to about 300% without permanent damage. Shear strain on the order of 100% is a common design criterion. Bearing diameters up to 1m and load capacities up to 5 MN are commercially available.

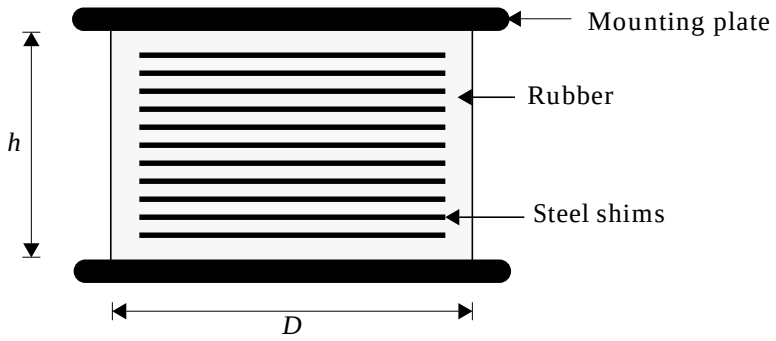

Fig. 5.12: Typical natural rubber bearing (NRB).

Rigidity under low level lateral loads

Increasing the lateral flexibility by incorporating a base isolation system provides an effective solution for high level seismic excitation. Although the relative motion between the structure and the support may be large, the absolute structural motion is generally small, so that the structure does not feel the earthquake. The effect of other types of lateral loading such as wind is quite different. In this case, the loading is applied directly to the structure, and the low lateral stiffness can result in substantial lateral displacement of the structure relative to the fixed support.

To control the motion under service loading, one can incorporate an additional stiffness system that functions for service loading but is not operational for high level loading. Systems composed of rods and / or springs that are designed to behave elastically up to a certain level of service loading and then yield have been developed and are commercially available. There are a variety of steel dampers having the above characteristics that can be combined with the rubber bearings. Figure 5.13 illustrate a particular scheme. The steel rod is dimensioned (length and area) such that it provides the initial stiffness and yields at the intended force level. The earliest solution and still the most popular approach is to incorporate a lead rod in the rubber bearing, as illustrated in Fig. 5.14. The lead plug is dimensioned according to the force level at which the system is intended to yield.

Fig. 5.13: Steel rod damper combined with a NRB.

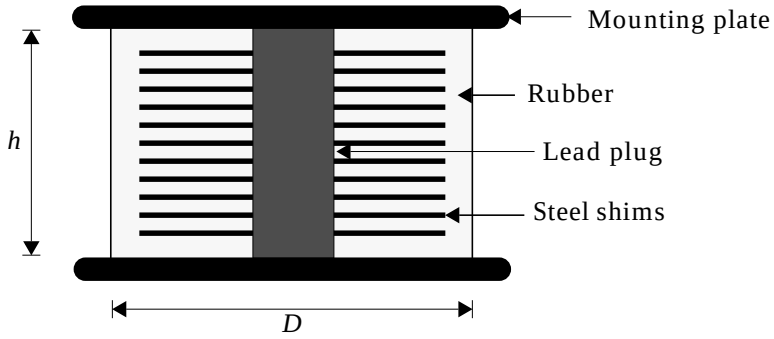

Fig. 5.14: Typical lead rubber bearing (LRB).

Energy dissipation/absorption

Rubber bearings behave in a viscoelastic manner and have some energy dissipation capacity. Additional damping can be provided by separate devices such as viscous, hysteretic, and friction dampers acting in parallel with the rubber bearings. The lead rubber bearing (LRB) is representative of this design approach; the lead plug provides both initial stiffness and hysteretic damping. Since hysteretic damping action occurs only at high level loading, hysteretic-type systems require additional viscous damping to control the response for low level loading. High damping natural rubber with a dissipation capacity about 4 times the conventional value is used together with other devices to improve the energy dissipation capacity of the isolation system. Figure 5.15 illustrates the deployment of a combination of NRB's, steel dampers, and viscous dampers. This scheme allows one to adjust both stiffness and damping for each load level, i.e., for both low and high level loading.

Fig. 5.15: Isolation devices of Bridgestone Toranomon Building.

Modeling of a natural rubber bearing (NRB)

For the purpose of preliminary design, a NRB can be modeled as a simple shear element having a cylindrical shape and composed of a viscoelastic material. Figure 5.16 defines the notation and shows the mode of deformation. The relevant equations are

$$\gamma = \frac{u}{h} \tag{5.49}$$

$$F = \tau A \tag{5.50}$$

$$h = n t_b \tag{5.51}$$

where A is the cross-sectional area, t_b is the thickness of an individual rubber sheet, and n is the total number of sheets. Each sheet is assumed to be in simple shear.

Applying the viscoelastic constitutive relations developed in Section 3.3, the behavior for harmonic shear strain is given by

$$\gamma = \hat{\gamma} \sin \Omega t \tag{5.52}$$

$$\tau = G_s \hat{\gamma} \sin \Omega t + \eta G_s \hat{\gamma} \cos \Omega t \tag{5.53}$$

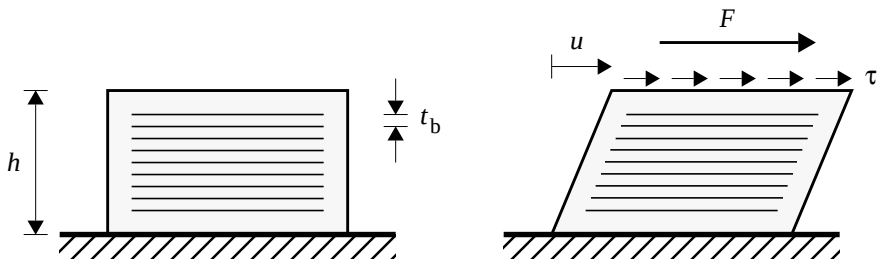

Fig. 5.16: Natural rubber bearing under horizontal loading.

where G_s is the storage modulus and η is the loss factor. In general, G_s and η are functions of the forcing frequency and temperature. They are also functions of the strain amplitude in the case of high damping rubbers which exhibit nonlinear viscoelastic behavior. Combining the above equations leads to

$$u = \hat{u} \sin \Omega t \tag{5.54}$$

$$F = f_d G_s \hat{u} [\sin \Omega t + \eta \cos \Omega t] \tag{5.55}$$

where

$$\hat{u} = \hat{\gamma} h = \hat{\gamma} n t_b \tag{5.56}$$

$$f_d = \frac{A}{h} = \frac{A}{n t_b} \tag{5.57}$$

Note that f_d depends on the bearing geometry whereas η and G_s are material properties.

The standard form of the linearized force-displacement relation is defined

by eqn (3.70)

$$F = k_{eq}u + c_{eq}\dot{u} \tag{5.58}$$

where k_{eq} and c_{eq} are the equivalent linear stiffness and viscous damping terms. Estimates for k_{eq} and c_{eq} can be obtained with a least squares approach. Assuming there are N material property data sets covering the expected range of strain amplitude and frequency, the resulting approximate expressions are eqns (3.74), (3.76), and (3.77) which are listed below for convenience.

$$k_{eq} = f_d\left[\frac{1}{N}\sum_{i=1}^{N} G_s(\Omega_i)\right] = f_d\,\widehat{G}_s \tag{5.59}$$

$$c_{eq} = \alpha k_{eq} \tag{5.60}$$

$$\alpha = \frac{\sum_{i=1}^{N}\left(\frac{G_s\eta}{\Omega}\right)_i}{\sum_{i=1}^{N} G_s(\Omega_i)} \tag{5.61}$$

Equation (5.58) is used in the MDOF analysis presented in a later section.

Figures 5.17 and 5.18 show that the material properties for natural and filled rubber are essentially constant for the frequency range of interest. Assuming G_s and η are constant, the equivalent properties reduce to

$$k_{eq} = f_d G_s \tag{5.62}$$

$$\alpha = \frac{\eta}{2\pi} T_{av} \tag{5.63}$$

where T_{av} is the average period for the excitation and G_s, η are the "constant" values.

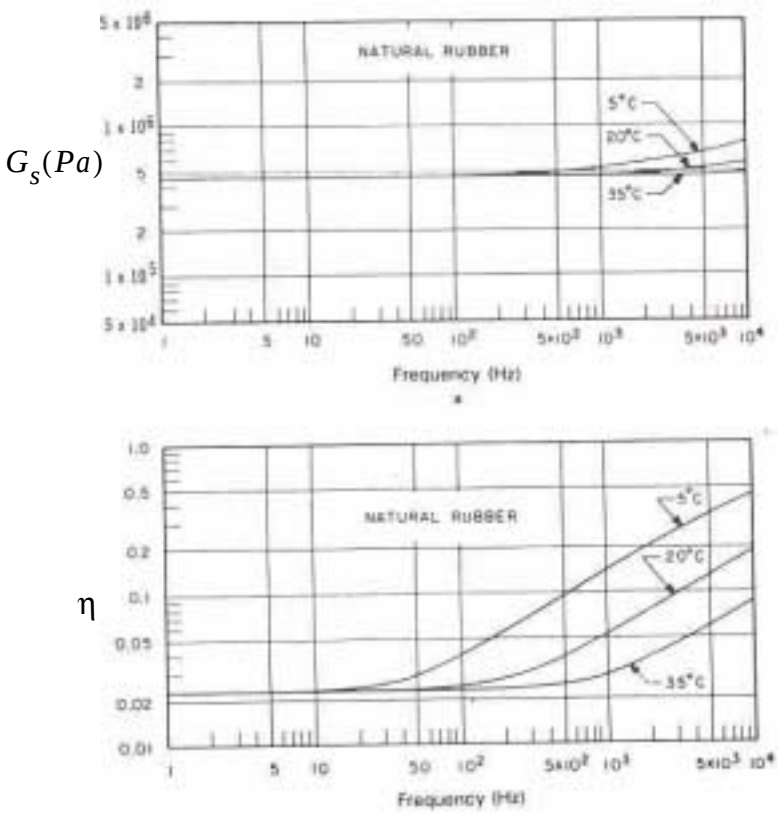

Fig. 5.17: Storage modulus and loss factor for natural rubber vs. frequency (Snowden, 1979)

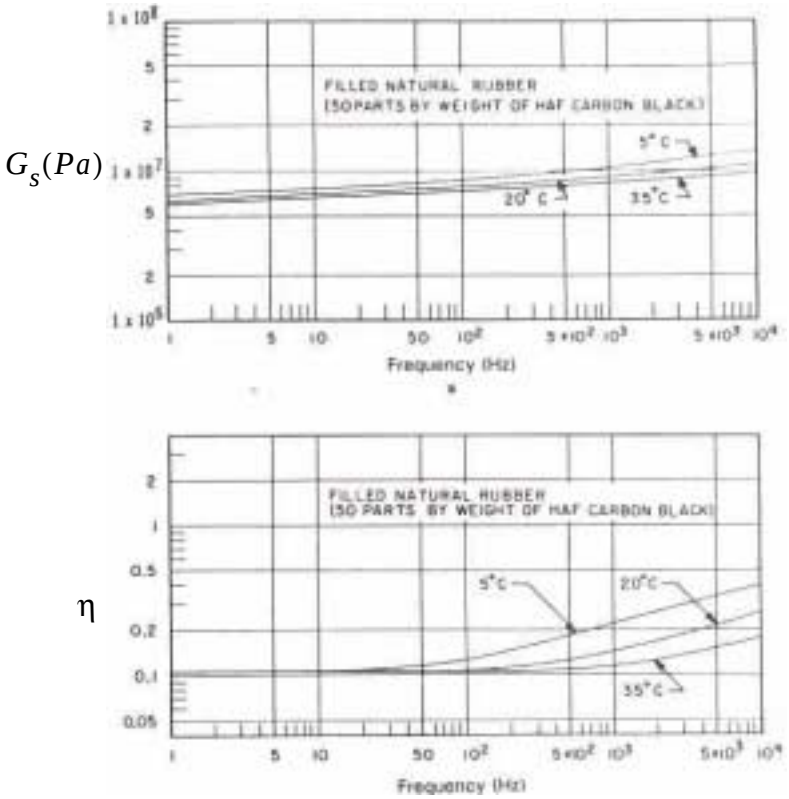

Fig. 5.18: Storage modulus and loss factor for filled natural rubber vs. frequency (Snowden, 1979)

Modeling of a lead rubber bearing (LRB)

As a first approximation, the LRB can be considered to consist of two elements: i) a linear viscoelastic element representing the rubber component, and ii) a linear elastic-perfectly plastic element simulating the lead plug. This model assumes that the static force response relationship is bilinear, as indicated in Fig. 5.19. The stiffness defined by eqn (5.62) can be used for the rubber bearing, i.e. for k_1.

$$k_{(rubber)} \equiv k_1 = f_d G_s \tag{5.64}$$

Considering lead to behave in a linear elastic manner, the plug stiffness can be expressed as

$$k_{(lead)} \equiv k_2 = \frac{A_p G_p}{h_p} \tag{5.65}$$

where A_p, h_p, and G_p denote the cross-sectional area, height, and shear modulus for the plug. Lastly, the displacement corresponding to the onset of yielding is related to the yield strain for lead by

$$u_y = h_p \gamma_y \tag{5.66}$$

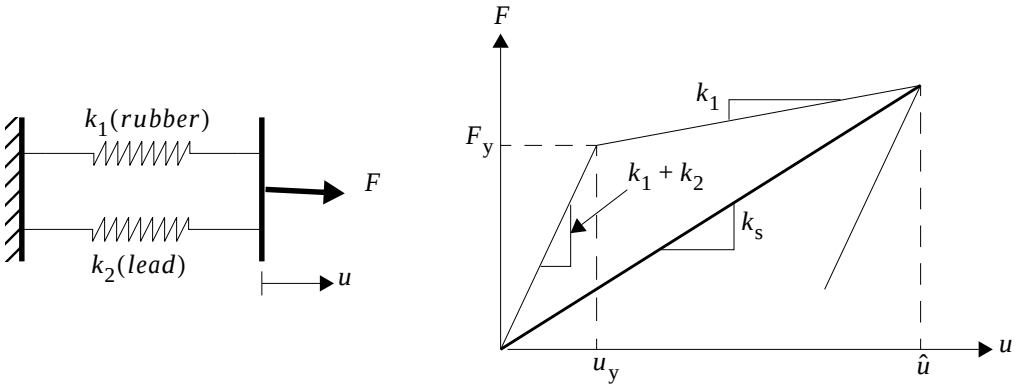

Fig. 5.19: Lead rubber bearing model - quasi static response.

Interpreting the behavior of the lead rubber bearing for large deformation as viscoelastic, the response due to harmonic motion is expressed in terms of a secant stiffness, k_s, and equivalent loss factor, $\tilde{\eta}$,

$$u = \hat{u} \sin \Omega t \tag{5.67}$$

$$F = k_s \hat{u} \sin \Omega t + \tilde{\eta} k_s \hat{u} \cos \Omega t \tag{5.68}$$

where k_s is related to the elastic energy storage capacity and $\tilde{\eta}$ is a measure of the energy dissipated through hysteretic damping of the rubber and lead components. Defining μ as the ductility ratio

$$\mu = \frac{\hat{u}}{u_y} = \frac{\hat{\gamma}}{\gamma_y} \tag{5.69}$$

the secant stiffness is related to the individual stiffness terms by

$$k_s = k_1 + \frac{k_2}{\mu} \tag{5.70}$$

The equivalent loss factor is defined as

$$\tilde{\eta} = \frac{1}{2\pi}\left[\frac{W}{E_S}\right] \tag{5.71}$$

where W is the hysteretic work per cycle and E_S is the maximum strain energy. Evaluating the energy terms

$$W = 4(\mu - 1)k_2 u_y^2 + \pi\eta k_1 \mu^2 u_y^2 \tag{5.72}$$

$$E_S = \frac{1}{2} k_s [\mu u_y]^2 \tag{5.73}$$

and substituting in eqn (5.71) leads to

$$\tilde{\eta} = \frac{4(\mu - 1)k_2}{\pi k_s \mu^2} + \eta\frac{k_1}{k_s} \tag{5.74}$$

Noting that γ_y is about 5×10^{-3} and the typical peak response strain is about 0.5, one can estimate μ as

$$\mu = \frac{\hat{\gamma}}{\gamma_y} \approx 100 \tag{5.75}$$

A typical value for the ratio of k_1 to k_2 is

$$k_1 \approx 0.1k_2 \tag{5.76}$$

Then, reasonable estimates for k_s and $\tilde{\eta}$ are

$$k_s = 1.1k_1 \tag{5.77}$$

$$\tilde{\eta} = \frac{4}{11\pi} + \frac{0.1}{0.11}\eta = 0.12 + 0.909\eta \tag{5.78}$$

The loss coefficient for high damping rubber can be as high as 0.15. Combining a

high damping rubber bearing with a lead plug provides an effective solution for both initial stiffness and damping over the range from low to high excitation.

The last step involves transforming eqn (5.68) to the standard form, eqn (5.58). Applying a least square approach and treating k_s and $\tilde{\eta}$ as functions of both the strain amplitude and frequency leads to

$$k_{eq} = \frac{1}{N}\sum_{i=1}^{N} k_s(\mu_i, \Omega_i) \tag{5.79}$$

$$c_{eq} = \frac{1}{N}\sum_{i=1}^{N} \frac{k_s(\mu_i, \Omega_i)\tilde{\eta}(\mu_i, \Omega_i)}{\Omega_i} \tag{5.80}$$

where N is the number of data sets, i.e., values of μ and Ω. It is reasonable to assume G_s and η are constant, and evaluate these parameters for a representative range of the ductility parameter, μ.

Applicability of base isolation systems

The feasibility of base isolation depends on whether it is needed, whether the proposed structure is suitable for base isolation, and whether it is cost effective compared with alternative solutions (Mayes *et al.* 1990). The need for base isolation may arise if the location is an area of high seismicity, if increased building safety and post earthquake operability are required, if reduced lateral design forces are desired, or if an existing structure needs upgrading to satisfy current safety requirements. A structure is considered suitable if: i) the subsoil conditions do not produce long period input motions to the structure, ii) the structure is less than about 10 to 15 stories and has a height-to-width ratio that prevents overturning, iii) the site permits the required level of motion of the base with respect to ground, and iv) the non-seismic lateral loads (such as wind) are less than approximately 10% of the weight of the structure.

The cost effectiveness of a base isolated structure can be assessed by assigning values to both the initial and life cycle costs and benefits. Examples of cost items are: the bearings, changes to accommodate the isolation system, maintenance and inspection of the isolation system, and the cost of maintaining

operability after earthquakes. Examples of savings are: lower initial cost of the structural system, less construction time, lower insurance premium, reduction in earthquake structural and nonstructural damage, and the reduction in injuries, deaths, and lawsuits from related damages. When disruption costs and the value of the building contents are important, seismic isolation has a substantial economic advantage over other systems provided that such an isolation scheme is technically feasible. Under such conditions, initial cost savings of up to 5% of the building cost have been noticed. For conventional buildings where disruption of operation is not important, there may not be sufficient cost savings in the structural system to offset the cost of the isolators (Mayes *et al.* 1990).

The greatest advantage of base isolation is achieved when it is considered in the early planning stages of the project, since it is possible to take advantage of the reduced response due to the isolation system. If the Base Isolation System is selected and added after completion of the structural design, many complications may arise since the construction techniques may have to be altered.

For bridge construction on the other hand, the economic issues are very different from those for buildings. In bridges, the implementation of seismic isolation simply requires the use of a seismic isolation bearing rather than a conventional bearing. Since bearings are only one or two percent of the cost of a bridge, an increase in the cost of isolation bearings will have very little impact on the overall construction cost and consequently, the use of a seismic isolation system is expected to reduce the overall construction cost (Billings *et al.* 1985).

5.4 *Examples of existing base isolation systems*

The past few years, especially since the Kobe earthquake in Japan, have seen a significant increase in the number of base isolated structures which suggests that the technology is gaining acceptance. A short description of some of the first implementations of base isolation systems is presented here to provide an indication of the type of buildings that are being isolated and the cost savings, if any, achieved by employing this technology. More comprehensive descriptions are contained in Kelly (1993), the Architectural Institute of Japan Guide to Base Isolated Buildings in Japan (1993), and various company web sites listed in the Electronic Reference Section of the text.

USC University Hospital (Myers 1989, Asher & Van Volkingburg 1989)

This eight-story structure, shown in Fig 5.20, is used as a teaching hospital by the University of Southern California. It resists seismic forces with a steel braced frame located on the perimeter, and is supported on 68 LRB and 81 NRB isolators. The seismic design was based on a 0.4*g* response spectrum increased by 20% to account for near-fault effects. The decision to incorporate seismic isolation was made in the preliminary design phase of the project. Structural cost comparisons for conventional and isolated structures were developed and the benefits of seismic isolation were assessed. It was determined that the cost savings in the structural frame would be sufficient to pay for the new structural ground floor slab and the isolation system. The additional cost of mechanical and architectural details was 1.3% and there was a 1.4% cost savings in the soil nailed retaining wall used in the isolation design versus the conventional retaining wall. Consequently, there was no net additional cost for incorporating seismic isolation on this hospital project.

Fig. 5.20: USC University Hospital

Fire Department Command and Control Facility (Mayes *et al.* 1990)

This is a two-story, steel perimeter braced frame structure that utilizes 36 high-damping elastomeric isolation bearings. The decision to utilize seismic isolation on this project was based on a comparison of two designs (conventional and isolation) that required maintaining the functionality of the structure after the extreme design event. This project reflects the first such detailed comparison for two designs to meet a performance specification. In the case of this two-story

structure, the isolated structure was found to be 6% less expensive than conventional design. A reduction in losses by a factor of 40 is expected with the seismic isolation.

Evans and Sutherland Manufacturing Facility (Reaveley *et al.* 1989)

The building, (see Fig 5.21), is a four-story manufacturing site for flight simulators located near the Warm Springs and East faults in Salt Lake City. The building measures 280ft x 160ft in plan and rests on 40 LRB and 58 NRB isolators. Preliminary costs for conventional and isolated designs were developed and the benefits of seismic isolation assessed at the conceptual design phase. The structural engineers decided to design the structural framing system for the UBC code forces for conventional design and, consequently, there were no structural framing cost savings. The additional structural cost was the basement structural floor (versus a slab-on-grade) and the heavy fail safe system used. Based on cost data developed by the contractors, the cost premium for incorporating seismic isolation was 5% or $400,000 on an $8 million project. Important in the decision to employ seismic isolation was protecting the building contents, including work in progress, the value of which exceeds $100 million (approximately 12 times the cost of the structure).

Fig. 5.21: Evans and Sutherland Facility

Salt Lake City Building (Mayes *et al.* 1987, Walters *et al.* 1986)

This facility, shown in Fig 5.22, is a five-story, Richardson Romanesque Revival structure constructed between 1892 and 1894, 265ft x 130ft in plan, and built of unreinforced brick and sandstone. Its 12 story tower is centrally located and is also constructed of unreinforced masonry. The building was restored and a combination of 208 LRB and 239 NRB isolators were installed, separating the building from its foundation. The structure is now protected against damage for the 0.2*g* design earthquake event. This project was the subject of a detailed study of several retrofit schemes among which were base isolation and UBC strengthening. The schemes were developed in sufficient detail to permit cost estimates and an evaluation of performance. Although the cost of these two alternatives was comparable, the decision to use seismic isolation was made based on the considerably better performance that results from the implementation of such a scheme. The complete architectural and historic restoration, and seismic rehabilitation work was estimated to be $24 million. The approximate value of the seismic isolation work reported by the contractor was $4,414,000 including the cost of the 447 seismic isolators.

Fig. 5.22: Salt Lake City Building

The Toushin 24 Ohmori Building (Kajima, 1989)

This building has 1 underground story which is used as a parking garage, and 9 stories above ground. It is located adjacent to 2 of the busiest railway lines in Tokyo, and the isolation system was required to reduce the traffic induced vibration as well as seismic motion. Figure 5.23 shows a view of the building, a

sectional plan, and the isolation scheme. A combination of laminated natural rubber bearings and steel rod dampers were deployed. Thick layers of rubber were used to decrease the vertical stiffness and thus filter out vertical micro-tremors.

a)View of building

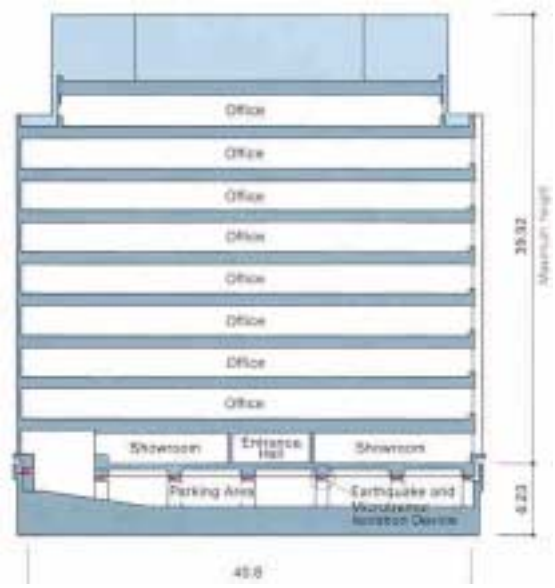

b) Section

c) Devices

Fig. 5.23: The Toushin 24 Ohmori Building

Bridgestone Toranomon Building (Shimizu, 1987)

The Bridgestone Toranomon Building (see Fig 5.24) is an office building of the Bridgestone Corporation, a major supplier of rubber products such as bearings. The base isolation system consists of 12 laminated rubber bearings, 25 steel dampers, and 8 viscous (oil) dampers. Figure 5.15 shows the layout of the devices. The viscous dampers are intended to dissipate the energy associated with wind and low intensity excitations. At this load level, the steel dampers are designed to behave elastically and provide stiffness. Energy associated with a large seismic excitation is dissipated / absorbed primarily by the steel dampers.

Fig. 5.24: Bridgestone Toranomon Building

San Francisco City Hall (1994)

San Francisco City Hall is an historic structure that is currently being

retrofitted with a seismic isolation system consisting of 530 lead rubber isolators. The design basis earthquake is 0.50g. Cost of retrofitting the structure is estimated at $105 million.

Fig. 5.25: San Francisco City Hall

Long Beach V.A. Hospital

The hospital is 12 story concrete structure with shear walls. A combination of 110 LRB, 18 NRB and 18 sliding bearings were installed in the mechanical crawl spaces below the building to improve the building's ability to survive earthquakes up to magnitude 0.32g.

Fig. 5.26: Long Beach V.A. Hospital

5.5 *Optimal stiffness distribution - discrete shear beam*

The theory developed earlier in this chapter for the SDOF case is extended here to deal with the more general case of a deformable beam-type structure supported by a base isolation system. Linear behavior is assumed since the objective is to generate results which are suitable for preliminary design. The approach followed to establish the stiffness distribution for the structure is similar to what was presented in Chapter 2. The only modification required is to include the effect of the stiffness and damping associated with the base isolation system. Most of the notation and relevant equations have been introduced in Chapter 2.

In what follows, the stiffness distribution corresponding to uniform deformation for the fundamental mode of the composite system consisting of a discrete shear beam and isolation system is derived. The theory is extended to deal with continuous beams in the next section.

Scaled stiffness distribution

Figure 5.27 defines the notation used for the base isolated shear beam. The bearing system is represented by an equivalent linear spring, k_1, and linear viscous damper, c_1; m_1 represents the mass lumped at the foundation level above the bearings; u_i is the displacement of the mass m_i with respect to the ground; k_i and c_i are the story stiffness and viscous damping coefficients for the actual structure. The governing equations for free undamped vibration are expressed as

$$\boldsymbol{M\ddot{U}} + \boldsymbol{KU} = \boldsymbol{0} \tag{5.81}$$

where the various matrices are the same as defined in chapter 2.

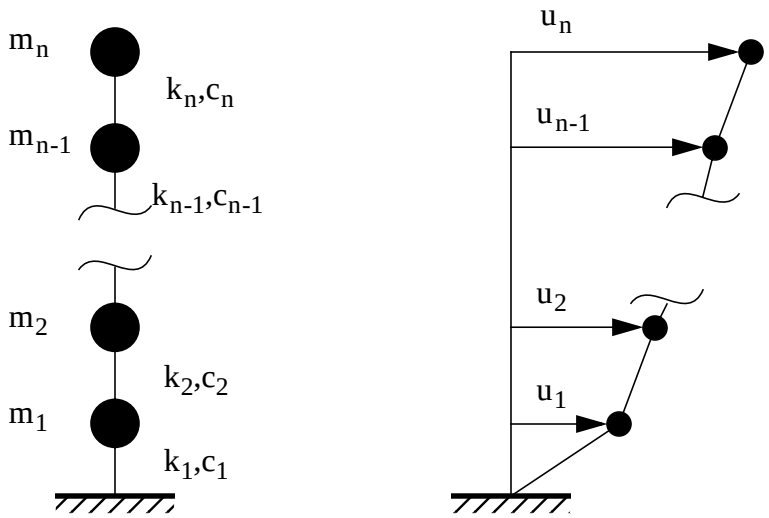

Fig. 5.27: Notations for base isolated discrete shear beam.

In the previous development, the modal displacement profile was selected such that the interstory displacement was constant over the beam. That strategy is modified here to allow for a different interstory displacement for the first story, which, in this model, represents the **relative displacement of the bearing**.

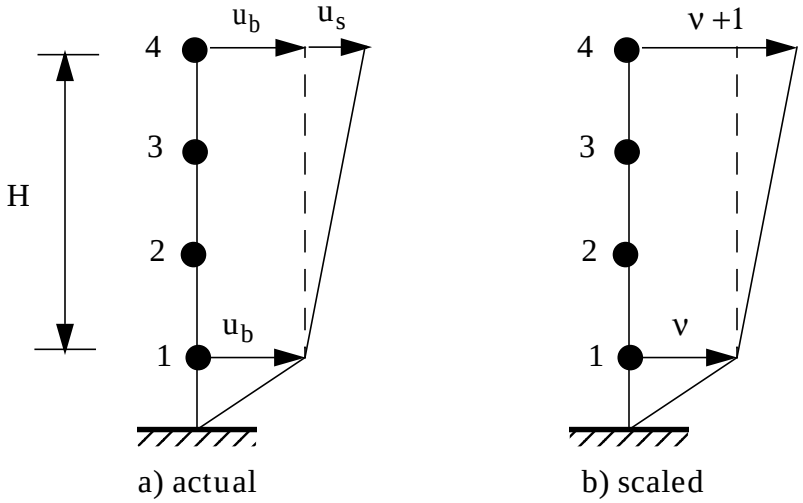

Fig. 5.28: Example displacement profile.

Figure 5.28a illustrates the choice of displacement profile; u_s is the displacement at the top node due to deformation of the beam, and u_b is the bearing displacement. For equal story height, the bilinear profile corresponds to uniform shear in the beam, $\gamma = u_s/H$. The bearing displacement is expressed as a multiple of the maximum structural displacement,

$$u_b = \nu\, u_s \tag{5.82}$$

and the profile is scaled by taking u_s as the independent displacement parameter. Fig 5.28b shows the scaled profile. With this choice of displacement parameter, the displacement vector takes the form

$$\begin{aligned} \mathbf{U} &= q\Phi \\ &= u_s\left\{\nu, \quad \nu+\frac{1}{3}, \quad \nu+\frac{2}{3}, \quad \nu+1\right\} \end{aligned} \tag{5.83}$$

Note that the choice of q as the maximum structural displacement due to deformation of the structure is consistent with the approach followed for the fixed base case. The modified displacement profile introduced here allows for an additional story at the bottom of the beam and distinguishes between the deformation at the base and within the beam.

Generalizing this approach for an n'th order system, the fundamental mode profile is taken as

$$\begin{aligned} \mathbf{U} &= q\Phi \\ \Phi &= \left\{\nu, \quad \nu+\frac{1}{n-1}, \quad \nu+\frac{2}{n-1}, \ldots, \quad \nu+1\right\} \end{aligned} \tag{5.84}$$

The remaining steps are the same as followed in section 2.7. One writes $\mathbf{U} = e^{\pm i\omega t}\Phi$ and substitutes for $\mathbf{U}$ in eqn (5.81). This leads to

$$\boldsymbol{K}\Phi = \omega^2 \boldsymbol{M}\Phi \tag{5.85}$$

Scaling **K** and rearranging the equations results in

$$\boldsymbol{Sk}' = \boldsymbol{M}\Phi \tag{5.86}$$

where $k'_i = k_i/\omega^2$ and **S** is defined by eqn (2.161), listed below for convenience.

$$\begin{aligned} \boldsymbol{S}'(i,i) &= \Phi_i - \Phi_{i-1} \\ \boldsymbol{S}'(i,i+1) &= \Phi_i - \Phi_{i+1} \\ \boldsymbol{S}'(i,j) &= 0 \text{ for } j \neq i, i+1 \end{aligned} \tag{5.87}$$

Given **M** and Φ, one solves eqn (5.86) for $\boldsymbol{k}'$. This procedure is illustrated with the following example.

Example 5.3: ***Scaled stiffness for a 4DOF beam with base isolation.***

Consider the beam shown in Fig 5.28. The various matrices are

$$\Phi = \left\{ \nu, \quad \nu + \frac{1}{3}, \quad \nu + \frac{2}{3}, \quad \nu + 1 \right\} \tag{1}$$

$$\boldsymbol{M}\Phi = \left\{ m_1\nu, \quad m_2\left(\nu + \frac{1}{3}\right), \quad m_3\left(\nu + \frac{2}{3}\right), \quad m_4(\nu + 1) \right\} \tag{2}$$

$$\boldsymbol{S} = \begin{bmatrix} \nu & -1/3 & & \\ & 1/3 & -1/3 & \\ & & 1/3 & -1/3 \\ & & & 1/3 \end{bmatrix} \tag{3}$$

$$\boldsymbol{k}' = \{k'_1 \quad k'_2 \quad k'_3 \quad k'_4\} \tag{4}$$

$$\begin{aligned} k'_4 &= 3m_4(\nu + 1) \\ k'_3 &= 3m_3\left(\nu + \frac{2}{3}\right) + k'_4 \\ k'_2 &= 3m_2\left(\nu + \frac{1}{3}\right) + k'_3 \\ k'_1 &= m_1 + \frac{k'_2}{3\nu} \end{aligned} \tag{5}$$

When the masses are equal, eqn (5) reduces to

$$
\begin{aligned}
k'_1 &= m^*\left(4+\frac{2}{\nu}\right)\\
k'_2 &= m^*(6+9\nu)\\
k'_3 &= m^*(5+6\nu)\\
k'_4 &= m^*(3+3\nu)
\end{aligned}
\tag{6}
$$

Fundamental mode response

Taking **U** according to eqn (5.84), the response of the fundamental mode is governed by

$$\tilde{m}\ddot{q}+\tilde{c}\dot{q}+\tilde{k}q = \tilde{p}-\tilde{m}\Gamma a_g \tag{5.88}$$

where the modal parameters are defined as

$$
\begin{aligned}
&\tilde{m} = \Phi^T\boldsymbol{M}\Phi \qquad \tilde{c} = \Phi^T\boldsymbol{C}\Phi \qquad \tilde{k} = \Phi^T\boldsymbol{K}\Phi\\
&\tilde{p} = \Phi^T\boldsymbol{P} \qquad \Gamma = \frac{\Phi^T\boldsymbol{M}\boldsymbol{E}}{\tilde{m}} \qquad \tilde{\xi} = \frac{\tilde{c}}{2\omega\tilde{m}}
\end{aligned}
\tag{5.89}
$$

Since Φ now involves the relative displacement factor, ν, these terms will also depend on ν.

Example 5.4:***Example 5.3 revisited.***

Modal parameters for the 4DOF shear beam considered in example 5.3 are listed below

$$\tilde{m} = m_1\nu^2 + m_2\left(\nu^2 + \frac{2}{3}\nu + \frac{1}{9}\right) + m_3\left(\nu^2 + \frac{4}{3}\nu + \frac{4}{9}\right) + m_4(\nu^2 + 2\nu + 1)$$

$$\Phi^T \boldsymbol{M}\boldsymbol{E} = m_1\nu + m_2\left(\nu + \frac{1}{3}\right) + m_3\left(\nu + \frac{2}{3}\right) + m_4(\nu + 1) \tag{1}$$

$$\tilde{c} = \nu^2 c_1 + \frac{1}{9}(c_2 + c_3 + c_4)$$

$$\tilde{p} = \nu p_1 + \left(\nu + \frac{1}{3}\right)p_2 + \left(\nu + \frac{2}{3}\right)p_3 + (\nu + 1)p_4$$

When the masses are equal, $\tilde{m}$ and Γ simplify to

$$\tilde{m} = m^*\left(4\nu^2 + 2\nu + \frac{14}{9}\right)$$

$$\Gamma = \frac{2\nu + 1}{2\nu^2 + \nu + \frac{7}{9}} = \frac{9}{7}\left[\frac{1 + 2\nu}{1 + \frac{9}{7}\nu(1 + 2\nu)}\right] \tag{2}$$

Values of $\tilde{m}/m^*$ and Γ for a range of values of ν are listed below in Table 5.1. There is a significant reduction in Γ with increasing ν, and this results in a reduced response to seismic excitation.

Table 5.1: Modal mass and participation factors for 4DOF shear beam with equal modal masses.

ν	$\tilde{m}/m^*$	Γ
0	1.556	1.286
1	7.556	0.794
2	21.556	0.464
3	43.556	0.321
4	73.556	0.245
5	111.556	0.197

The modal damping parameter, $\tilde{c}$, depends on both the bearing damping c_1 and the structural damping (c_2, c_3, c_4) properties. Incorporating damping in the bearing is more effective than distributing damping over the structure for the

fundamental mode response. Structural damping is needed mainly to control the higher modes.

Stiffness calibration for seismic isolation

The peak fundamental mode response due to seismic excitation is given by

$$q_{max} = \frac{1}{\omega}\Gamma S_v(\omega, \xi) \tag{5.90}$$

One specifies q_{max}, ξ, and $S_v(\omega, \xi)$, and determines ω by iterating on eqn (5.90). By definition, q_{max} is the maximum structural displacement relative to the base motion due to deformation of the structure. It is evaluated using the design value for the maximum transverse shear strain and the structural height,

$$q_{max} = \gamma^* H \tag{5.91}$$

The peak amplitude of the bearing displacement relative to the ground follows from eqn (5.82)

$$u_b\big|_{max} \equiv u_1\big|_{max} = \nu q_{max} \tag{5.92}$$

Given q_{max} and $u_b\big|_{max}$, ν is determined with eqn (5.92). This approach has to be modified when the structure is taken to be rigid, i.e., when $q_{max} \approx 0$. In this case, the system reduces to a SDOF model, and the formulation presented in section 5.2 is applicable.

Example 5.5:*Stiffness calibration for Example 5.4*

Returning to the 4DOF example structure, the following data is assumed.

$$\begin{aligned} H &= 15m \\ \gamma^* &= 1/200 \\ S_v(\omega, \xi) &\ \textit{defined}\ \text{by Fig 5.29} \end{aligned} \tag{1}$$

Using (1),

$$q_{max} = (15)(1/200) = 0.075m \tag{2}$$

To proceed further, one needs to specify ν. Various cases are considered below.

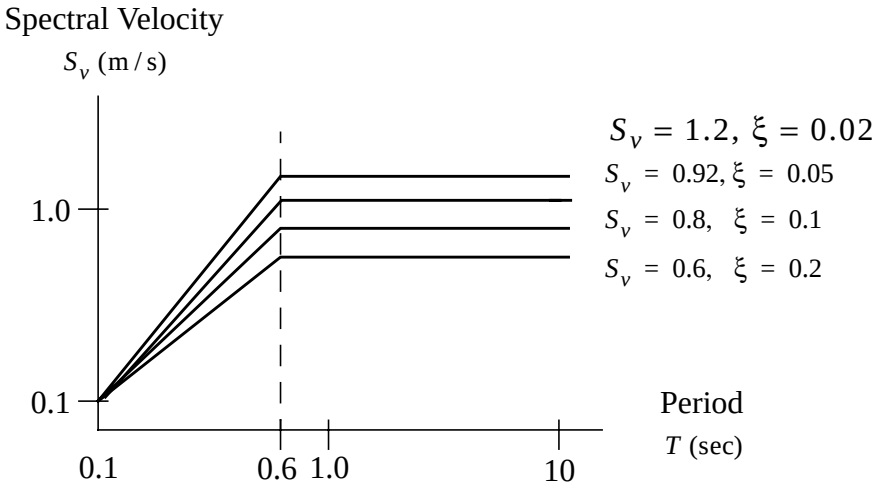

Fig. 5.29: Spectral velocity.

Case 1 $u_b\big|_{max} = 0.3m$

The parameters corresponding to this bearing displacement are

$$\begin{aligned} \nu &= 0.3/0.075 = 4 \\ \Gamma &= 0.245 \end{aligned} \tag{3}$$

Substituting in eqn (5.90) leads to an expression for the period, T.

$$T = \frac{2\pi q_{max}}{\Gamma S_v(T,\xi)} = \frac{1.922}{S_v(T,\xi)} \tag{4}$$

Suppose $\xi = 0.05$. From Fig 5.29, $S_v = 0.92$ for T>0.6 sec. No iteration is required here, since eqn (4) predicts T>0.6.

$$T = \frac{1.922}{0.92} = 2.13s$$
$$\omega = \frac{2\pi}{T} = 2.94r/s \tag{5}$$

The stiffness coefficients are generated using the results contained in example 5.3. For the case of uniform mass, eqns (7) of example 5.3 apply. Taking $\nu = 4$ and ω according to eqn (5) above leads to

$$k_4 = 129.6m^* \qquad k_3 = 244.6m^*$$
$$k_2 = 354.3m^* \qquad k_1 = 37.9m^* \tag{6}$$

Damping is determined with eqn (3) of example 5.4. For $\nu = 4$ and $\xi = 0.05$,

$$\tilde{m} = 111.6m^* \tag{7}$$

$$\tilde{c} = 2\xi\omega\tilde{m} = 2(0.05)(2.94)(111.6m^*) = 32.8m^* \tag{8}$$

The individual damping coefficients are related to $\tilde{c}$ by

$$\tilde{c} = 16c_1 + \frac{1}{9}(c_2 + c_3 + c_4) = 32.8m^* \tag{9}$$

One has to decide how to allocate damping to the various components. For example, assuming 75% of $\tilde{c}$ is contributed by the bearing requires

$$c_1 = 1.54m^*$$
$$c_2 + c_3 + c_4 = 73.8m^* \tag{10}$$

Placing damping at the base is an order of magnitude more effective than distributing the damping throughout the structure for this degree of isolation.

Case 2 $u_b\big|_{max} = 0.15m$

For this case, $\nu = 2$. The various parameters for $\xi = 0.05$, $\nu = 2$, and uniform mass are as follows.

$$
\begin{aligned}
&\Gamma = 0.464 \\
&T = 1.025s \\
&\omega = 6.16r/s \\
&\tilde{m} = 21.556m^* \\
&\tilde{c} = 13.28m^* \\
&4c_1 + \frac{1}{9}(c_2 + c_3 + c_4) = 13.28m^* \\
&k_4 = 341m^* \qquad k_3 = 644m^* \\
&k_2 = 909m^* \qquad k_1 = 189m^*
\end{aligned}
\tag{11}
$$

Case 3 Fixed base

The fixed base case is treated in examples 2.9 and 2.10. Specializing these results for uniform mass and $\xi = 0.05$ results in the following parameters and properties.

$$
\begin{aligned}
&\Gamma = 1.286 \\
&T = 0.5s \\
&\omega = 12.56r/s \\
&\tilde{m} = 1.556m^* \\
&\frac{1}{9}(c_2 + c_3 + c_4) = 1.95m^* \\
&k_4 = 473m^* \\
&k_3 = 788m^* \\
&k_2 = 946m^* \\
&k_1 = \infty
\end{aligned}
\tag{12}
$$

5.6 *Optimal stiffness distribution - continuous cantilever beam*

Stiffness distribution - undamped response

The equilibrium equations for undamped motion of the base isolated continuous beam shown in Fig. 5.30 are

$$V(x, t) = -\rho_m \int_x^H \ddot{u}(x, t)\,\mathrm{d}x \tag{5.93}$$

$$M(x, t) = \int_x^H V(x, t)\,\mathrm{d}x \tag{5.94}$$

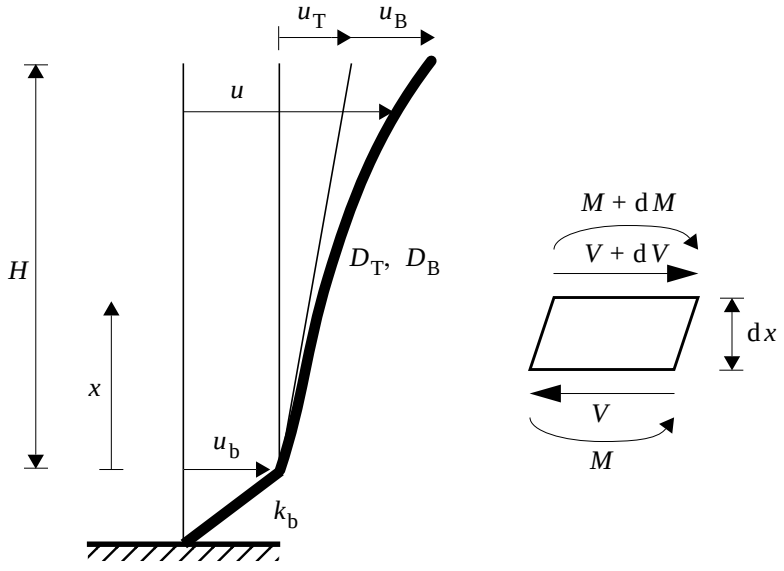

Fig. 5.30: Base isolated continuous beam.

The transverse shear and bending deformation measures for the beam are related to the translation and rotation quantities by

$$\frac{\partial u}{\partial x} = \gamma + \beta \tag{5.95}$$

$$\chi = \frac{\partial \beta}{\partial x} \tag{5.96}$$

Considering γ and χ to be functions only of time, integrating the resulting equations with respect to x, and imposing the boundary conditions at $x = 0$, one obtains expressions for u and β in terms of $\gamma(t)$, $\chi(t)$, and $u_b(t)$

$$u = \gamma x + \frac{1}{2}\chi x^2 + u_b \tag{5.97}$$

$$\beta = \chi x \tag{5.98}$$

where u_b denotes the displacement of the base of the structure with respect to ground. Taking

$$\gamma = \gamma^* e^{i\omega_1 t} \tag{5.99}$$

$$\chi = \chi^* e^{i\omega_1 t} \tag{5.100}$$

$$u_b = u_b^* e^{i\omega_1 t} \tag{5.101}$$

produces a periodic motion of the beam. Noting that the deformation measures γ^* and χ^* are related by (see eqn (2.14) and Fig 5.30)

$$s = \frac{u_B}{u_T} = \frac{\chi^* H}{2\gamma^*} \tag{5.102}$$

and expressing u_b^* in terms of the displacement at $x = H$ due to shear deformation (see Fig. 5.30)

$$u_b^* = \nu u_T^* = \nu \gamma^* H \tag{5.103}$$

transforms eqn (5.97) into

$$u = \left(\frac{x}{H} + \frac{s x^2}{H^2} + \nu\right)\gamma^* H e^{i\omega_1 t} = \Phi(x)\,(\gamma^* H e^{i\omega_1 t}) = q(t)\Phi(x) \tag{5.104}$$

The function $\Phi(x)$ defines the fundamental mode. The corresponding expression

for the fixed base case is eqn (2.189).

Differentiating u with respect to time,

$$\ddot{u} = -\left(x + \frac{sx^2}{H} + \nu H\right)\gamma^* \omega_1^2 e^{i\omega_1 t} \tag{5.105}$$

and substituting for $\ddot{u}$ in eqn (5.93) leads to

$$V = \rho_m \omega_1^2 H^2 \left(\frac{1}{2} + \frac{s}{3} + \nu - \frac{x^2}{2H^2} - \frac{sx^3}{3H^3} - \frac{\nu x}{H}\right)\gamma^* e^{i\omega_1 t} \tag{5.106}$$

The corresponding relation for the bending moment is

$$M = \rho_m \omega_1^2 H^4 \chi^* e^{i\omega_1 t}\left[\frac{1}{6s} + \frac{1}{8} + \frac{\nu}{4s} - \left[\frac{1}{4s} + \frac{1}{6} + \frac{\nu}{2s}\right]\frac{x}{H} + \frac{\nu x^2}{4sH^2} + \frac{x^3}{12sH^3} + \frac{x^4}{24H^4}\right] \tag{5.107}$$

Lastly, the shear and bending rigidity distributions are determined with the definition equations

$$D_T = \frac{V}{\gamma^*} = \rho_m \omega_1^2 H^2 \left[\frac{1}{2} + \frac{s}{3} + \nu - \frac{x^2}{2H^2} - \frac{sx^3}{3H^3} - \frac{\nu x}{H}\right] \tag{5.108}$$

$$D_B = \frac{M}{\chi^*} = \rho_m \omega_1^2 H^4 \left[\frac{1}{6s} + \frac{1}{8} + \frac{\nu}{4s} - \left(\frac{1}{4s} + \frac{1}{6} + \frac{\nu}{2s}\right)\frac{x}{H} + \frac{\nu x^2}{4sH^2} + \frac{x^3}{12sH^3} + \frac{x^4}{24H^4}\right] \tag{5.109}$$

Equation (5.108) is written as

$$D_T = \frac{D_T(0)}{\left[\frac{1}{2} + \frac{s}{3} + \nu\right]}\left(\frac{1}{2} + \frac{s}{3} + \nu - \frac{x^2}{2H^2} - \frac{sx^3}{3} - \frac{\nu x}{H}\right) \tag{5.110}$$

where $D_T(0)$ is the shear rigidity at the base.

$$D_T(0) = \rho_m \omega_1^2 H^2 \left(\frac{1}{2} + \frac{s}{3} + \nu\right) \equiv k_s H \tag{5.111}$$

The parameter, k_s, can be interpreted as an equivalent shear stiffness

measure.The shear force at the base of the beam must equal the shear force in the bearing to satisfy the force equilibrium condition for undamped motion. Equating these forces

$$D_{\mathrm{T}}(0)\gamma^* = k_{\mathrm{b}} u_{\mathrm{b}}^* = k_{\mathrm{b}} \nu \gamma^* H \tag{5.112}$$

and solving for k_b results in

$$k_{\mathrm{b}} = \frac{D_{\mathrm{T}}(0)}{\nu H} = \frac{1}{\nu} k_s \tag{5.113}$$

The fundamental frequency follows from eqn (5.111)

$$\omega_1^2 = \frac{D_{\mathrm{T}}(0)}{\rho_m H^2 \left(\frac{1}{2} + \frac{s}{3} + \nu \right)} \tag{5.114}$$

Figures 5.31 and 5.32 shows the mode shapes and shear deformation profiles for the first five modes of a typical low rise building. The variation in the mode shape profiles with the ratio of the stiffness of the isolator, k_{b}, to the shear beam stiffness k_s are illustrated by Figures 5.33, 5.34 and 5.35. This ratio is equal to $1/\nu$. Figure 5.36 displays the variation in the periods of the highest three fundamental modes. The primary influence is on the period of the fundamental mode which is significantly increased when the stiffness of the isolator is several orders of magnitude lower than the beam stiffness. The effect on the periods of the second and third modes is relatively insignificant. Figure 5.37 shows the variation of the participation of the second and third modes relative to the first. The plot shows that the contribution of the second and third modes is also significantly reduced by decreasing the stiffness of the isolator with respect to the beam stiffness.

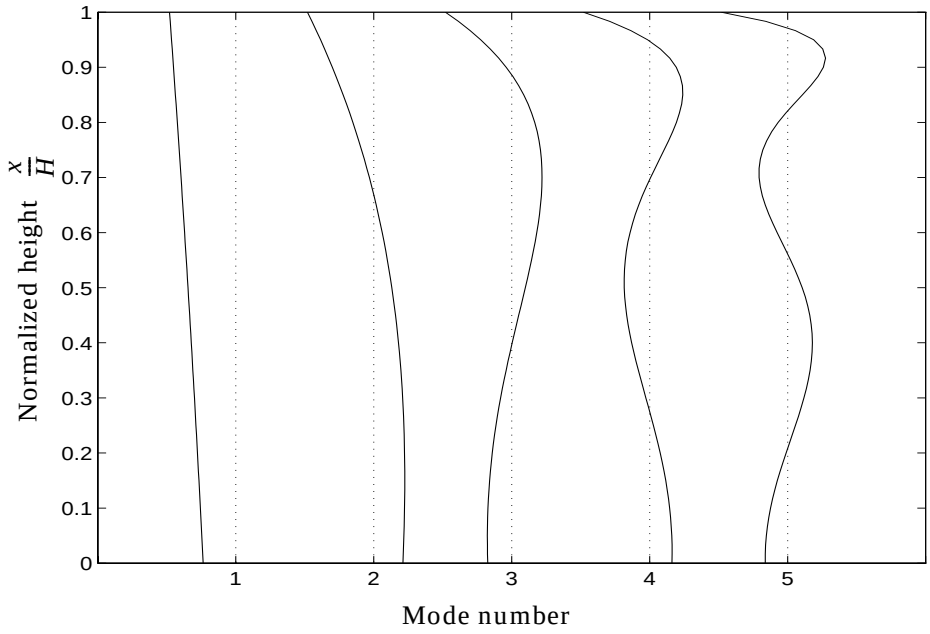

Fig. 5.31: Mode shapes for a typical base isolated structure.

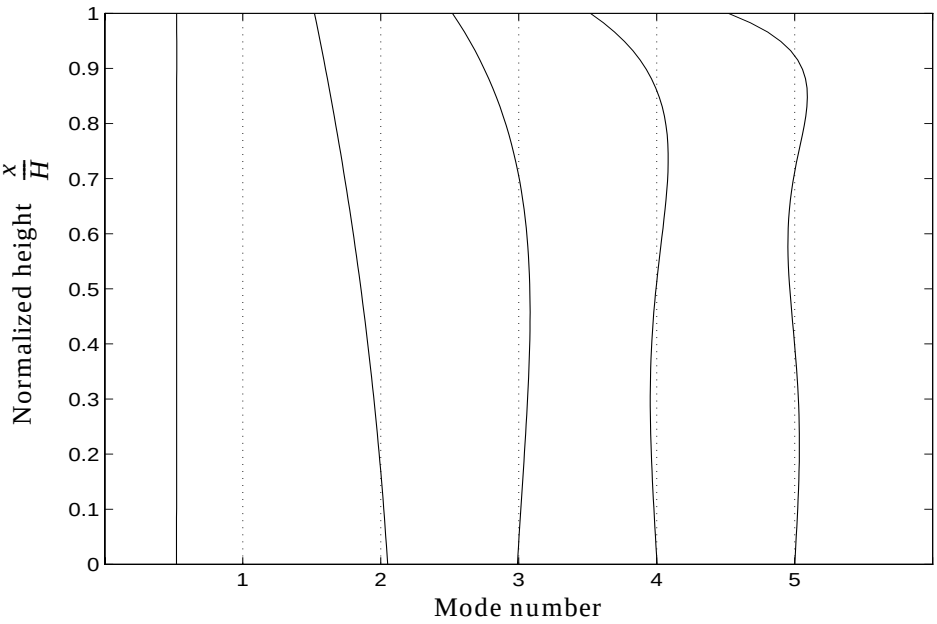

Fig. 5.32: Mode deformation profiles for a typical base isolated structure.

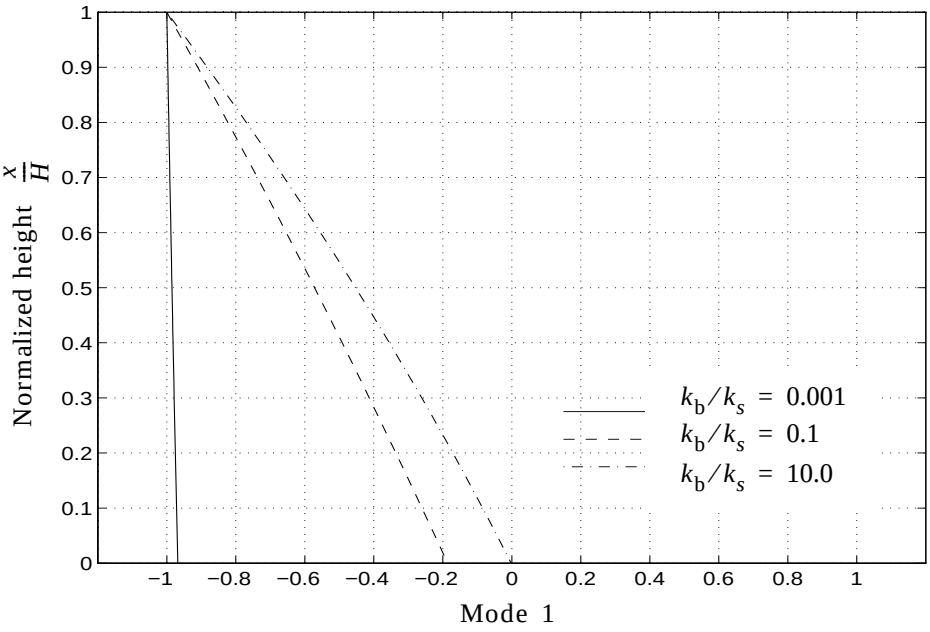

Fig. 5.33: Variation of mode 1 shape with relative stiffness of isolator.

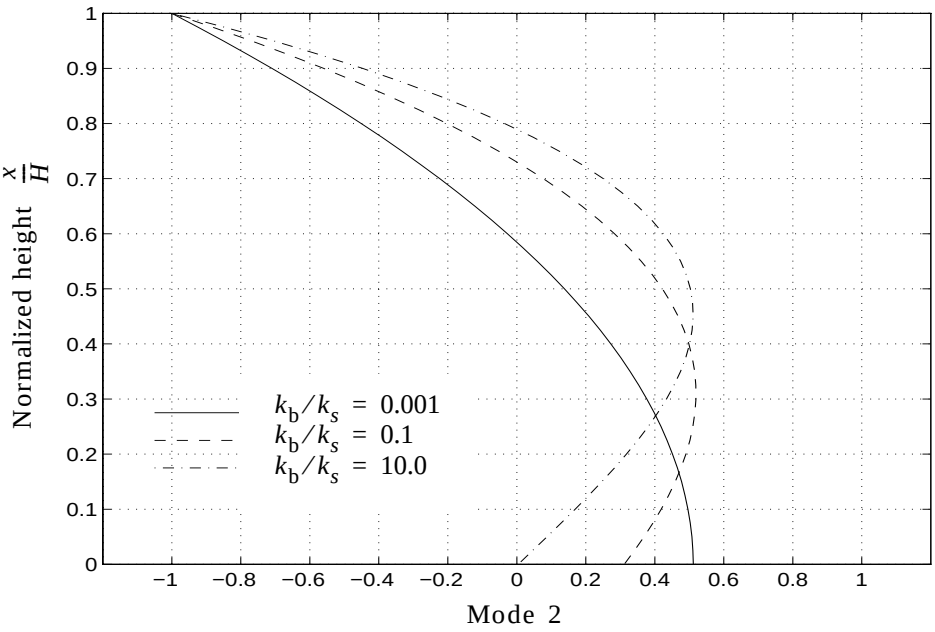

Fig. 5.34: Variation of mode 2 shape with relative stiffness of isolator.

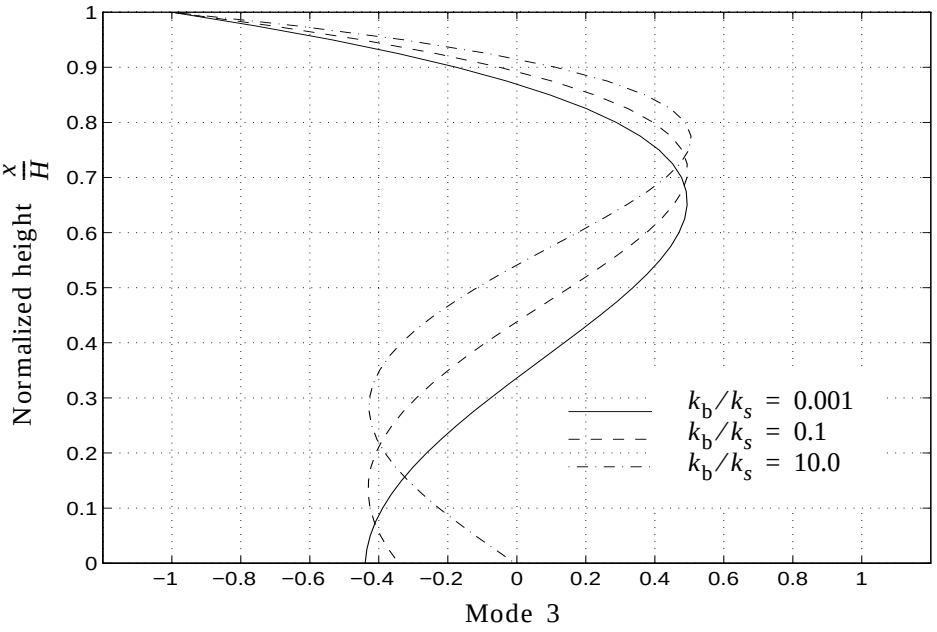

Fig. 5.35: Variation of mode 3 shape with relative stiffness of isolator.

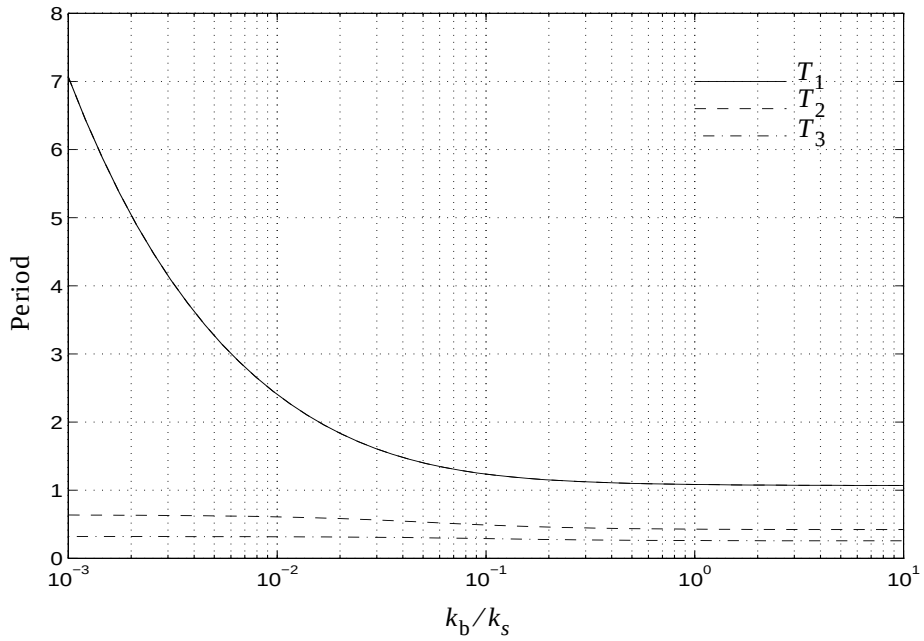

Fig. 5.36: Variation of periods with relative stiffness of isolator.

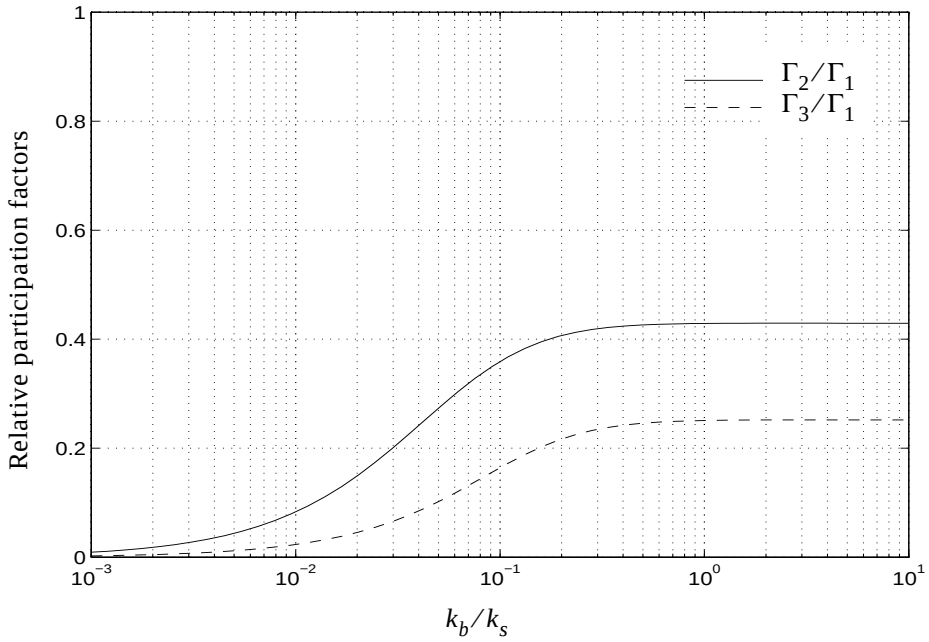

Fig. 5.37: Variation of relative participation factors with relative stiffness of isolator.

Fundamental mode equilibrium equation

Incorporating the contribution of the base isolation system, the principle of virtual displacements has the form

$$\int_0^H (M \cdot \delta\chi + V \cdot \delta\gamma)\,\mathrm{d}x + F_\mathrm{b} \cdot \delta u_\mathrm{b} = \int_0^H (b \cdot \delta u)\,\mathrm{d}x \tag{5.115}$$

where F_b is the shear force in the bearing. The equations relating internal forces to deformations and deformation rates are taken as

$$V = D_\mathrm{T}\gamma + C_\mathrm{T}\dot{\gamma} \tag{5.116}$$

$$M = D_\mathrm{B}\chi + C_\mathrm{B}\dot{\chi} \tag{5.117}$$

$$F_\mathrm{b} = k_\mathrm{b}u_\mathrm{b} + c_\mathrm{b}\dot{u}_\mathrm{b} \tag{5.118}$$

The form of the modal expansion follows from eqn (5.104).

$$u = q\Phi(x) = q\left(\frac{x}{H} + \frac{sx^2}{H^2} + \nu\right) \tag{5.119}$$

$$\beta = q\Psi(x) = q\left(\frac{2sx}{H^2}\right) \tag{5.120}$$

Assuming external loading and seismic excitation, the loading term is

$$b = -\rho_m a_g - \rho_m \ddot{u} + \bar{b}(x, t) \tag{5.121}$$

Finally, introducing the various terms in the principle of virtual displacements leads to the equilibrium equation for q

$$\tilde{m}\ddot{q} + \tilde{c}\dot{q} + \tilde{k}q = \tilde{p} \tag{5.122}$$

where

$$\tilde{m} = \int_0^H \rho_m \left[\frac{x}{H} + \frac{sx^2}{H^2} + \nu\right]^2 dx = \rho_m H\left[\frac{1}{3} + \nu + \nu^2 + \frac{s}{2} + \frac{2s\nu}{3} + \frac{s^2}{5}\right] \tag{5.123}$$

$$\tilde{c} = \int_0^H \left[\frac{C_T}{H^2} + \frac{4s^2 C_B}{H^4}\right] dx + c_b \nu^2 \tag{5.124}$$

$$\tilde{k} = \int_0^H \left[\frac{D_T}{H^2} + \frac{4s^2 D_B}{H^4}\right] dx + k_b \nu^2 \tag{5.125}$$

$$\tilde{p} = \int_0^H (\bar{b} - \rho_m a_g)\left[\frac{x}{H} + \frac{sx^2}{H^2} + \nu\right] dx = -\rho_m H\left[\frac{1}{2} + \nu + \frac{s}{3}\right] a_g - \tilde{p}_e \tag{5.126}$$

Expressing $\tilde{c}$ and $\tilde{k}$ as

$$\tilde{c} = 2\xi\omega\tilde{m} \tag{5.127}$$

$$\tilde{k} = \omega^2\tilde{m} \tag{5.128}$$

transforms eqn (5.122) to

$$\ddot{q} + 2\xi\omega\dot{q} + \omega^2 q = -\Gamma a_g + \frac{1}{\tilde{m}}\tilde{p}_e \tag{5.129}$$

where

$$\Gamma = \frac{\nu + \frac{1}{2} + \frac{s}{3}}{\frac{1}{3} + \nu^2 + \nu + \frac{s^2}{5} + \frac{s}{2} + \frac{2s\nu}{3}} \tag{5.130}$$

For a pure shear beam, $s = 0$ and the participation factor for the fundamental mode reduces to

$$\Gamma = \frac{\nu + \frac{1}{2}}{\frac{1}{3} + \nu^2 + \nu} \tag{5.131}$$

The expression for the modal damping ratio depends on how one specifies the damping over the beam.

Rigidity calibration - seismic excitation

The calibration procedure presented in Chapter 2 is applied to the base isolated model. Starting with

$$q_{max} = \frac{\Gamma S_v(\omega, \xi)}{\omega} \tag{5.132}$$

and substituting for q_{max} results in

$$\omega = \frac{\Gamma S_v}{\gamma^* H} = \frac{\nu\Gamma S_v}{u_b^*} \tag{5.133}$$

One specifies ν in addition to the other parameters (γ^*, ξ, S_v), and solves for ω . This value is then used to determine $D_T(0)$ and k_b with eqns (5.111) and (5.113).

Example 5.6:*Stiffness calibration - Example Building #2.*

The stiffness calibration for Building example #2 was considered in Chapter 2. In what follows, the calibration procedure is extended to include stiffness and damping components located at the base. The design data are:

$$\begin{aligned} H &= 50m & \rho_m &= 20,000 kg/m \\ \gamma^* &= 1/200 & s &= 0.25 \\ \xi_1 &= 0.05 & S_v &= 0.92 m/s \end{aligned} \qquad (1)$$

Using (1), the peak relative structural displacement is

$$q_{max} = \gamma^* H = 0.25m \qquad (2)$$

To proceed further, one needs to specify the base displacement and then establish the value of ν with eqn (5.103). We take

$$u_b = 0.25m \qquad (3)$$

Then

$$\nu = \frac{u_b}{q_{max}} = 1.0 \qquad (4)$$

Given ν , the participation factor follows from eqn (5.130)

$$\Gamma = 0.600 \qquad (5)$$

The modal mass is determined with eqn (5.123)

$$\tilde{m} = 2.638 \times 10^6 kg \qquad (6)$$

Assuming C_T = constant and C_B =0 in eqn (5.124), the modal damping

coefficient reduces to

$$\tilde{c} = \frac{C_T}{H} + \nu^2 c_b = 0.02 C_T + c_b \tag{7}$$

Equation (5.127) relates $\tilde{c}$ to ω.

$$\tilde{c} = 2\xi\omega\tilde{m} = 0.2638 \times 10^6 \omega \quad Ns/m \tag{8}$$

Lastly, the frequency is found using eqn (5.133) and the design data for S_v ($\xi = 0.05$ and $S_v = 0.92 m/s$)

$$\begin{aligned} \omega &= \frac{\Gamma S_v}{\gamma^* H} = 2.4 S_v = 2.61 r/s \\ T &= 2.41 \text{sec} \end{aligned} \tag{9}$$

With ω known, the modal damping coefficient follows from eqn (8),

$$\tilde{c} = 0.688 MNs/m \tag{10}$$

and the transverse shear rigidity at the base of the beam is determined with eqn (5.111).

$$D_T(0) = 538.6 MN \tag{11}$$

Finally, given $D_T(0)$, the isolation stiffness is estimated using eqn (5.113), which is based on neglecting the contribution of the damping force in the bearing.

$$k_b = 10.77 MN \tag{12}$$

5.7 *Building design examples*

Stiffness distribution based on fundamental mode response

Since base isolation is a potential solution for buildings with less than about 10 stories and having an aspect ratio that prevents overturning, only Buildings 1 and

2 of Chapter 2 are considered in the simulation. Tables 2.4 and 2.5 lists the design data. The damping in the structure is obtained by specifying ξ_1 and computing a stiffness proportional damping matrix considering a fixed based structure, as carried out in Chapter 2. The damping in the bearing for specified bearing damping ratio ξ_b is obtained by assuming the structure to be a SDOF system having a mass equal to the total mass of the structure and a stiffness equal to the stiffness of the bearing as obtained from eqn (5.113). Figures 5.38 and 5.39 show the shear rigidity distributions for Buildings 1 and 2 obtained with eqns (5.108) and (5.109), taking $S_v = 1.2\text{m/s}$. The corresponding shear deformation profiles for different combinations of building damping ratios and isolator damping ratios when the structures are subjected to scaled versions (to $S_v = 1.2\text{m/s}$ for $\xi = 0.02$) of the El Centro and Taft accelerograms are plotted in Figures 5.40 through 5.47. The maximum deformation in the bearing is also indicated on the plots. The plots show that increasing the damping in the bearing tends to reduce the bearing deformation without significantly altering the shape of the deformation profile along the structure's height. Furthermore, just as for the fixed base structures, the contribution of the higher modes becomes more significant as the structure becomes more slender. The structural parameters, as well as the mean and standard deviation results for the deformations of the above buildings are tabulated in the following section.

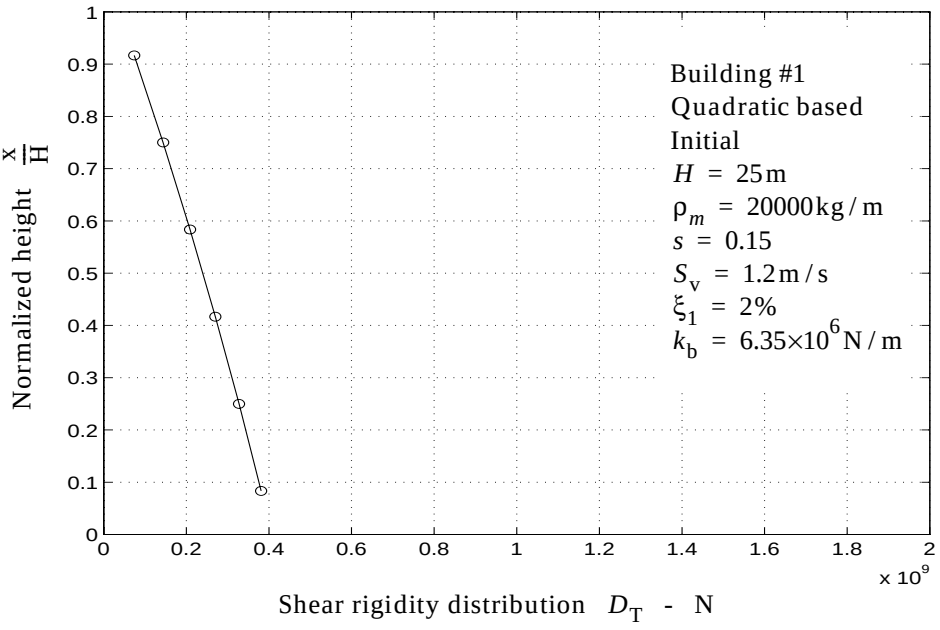

Fig. 5.38: Initial shear rigidity distribution for Building 1.

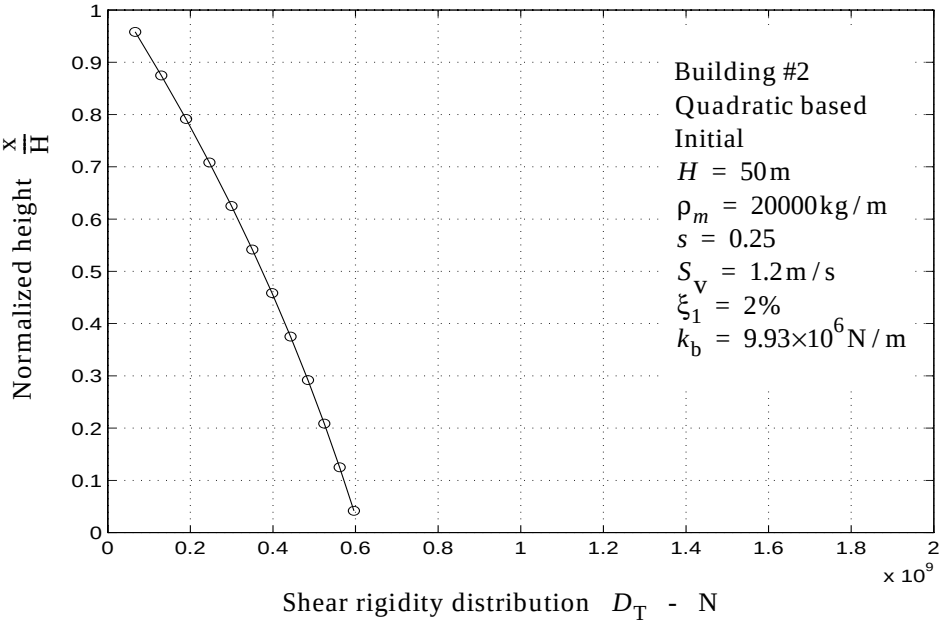

Fig. 5.39: Initial shear rigidity distribution for Building 2.

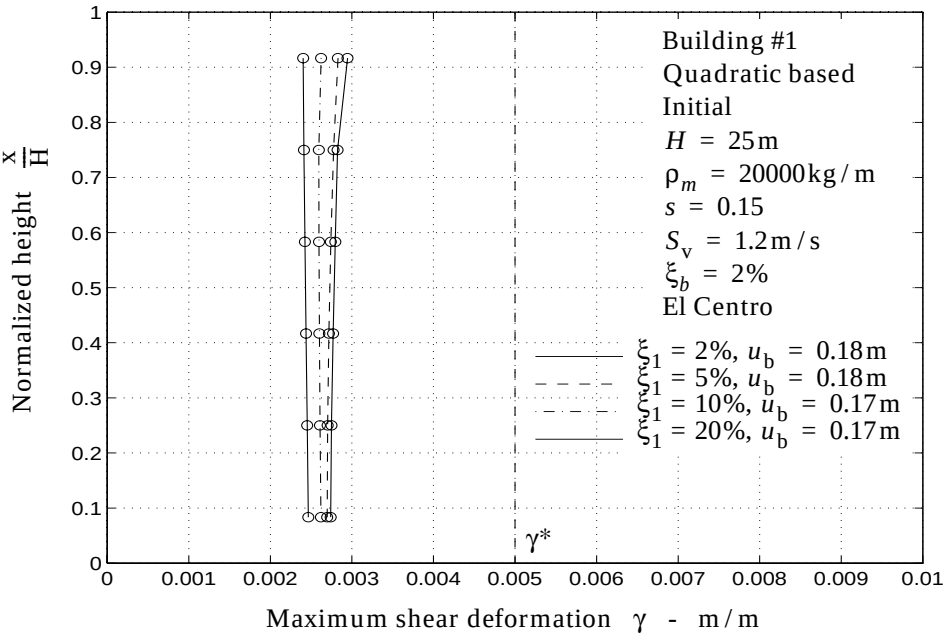

Fig. 5.40: Maximum shear deformation for Building 1.

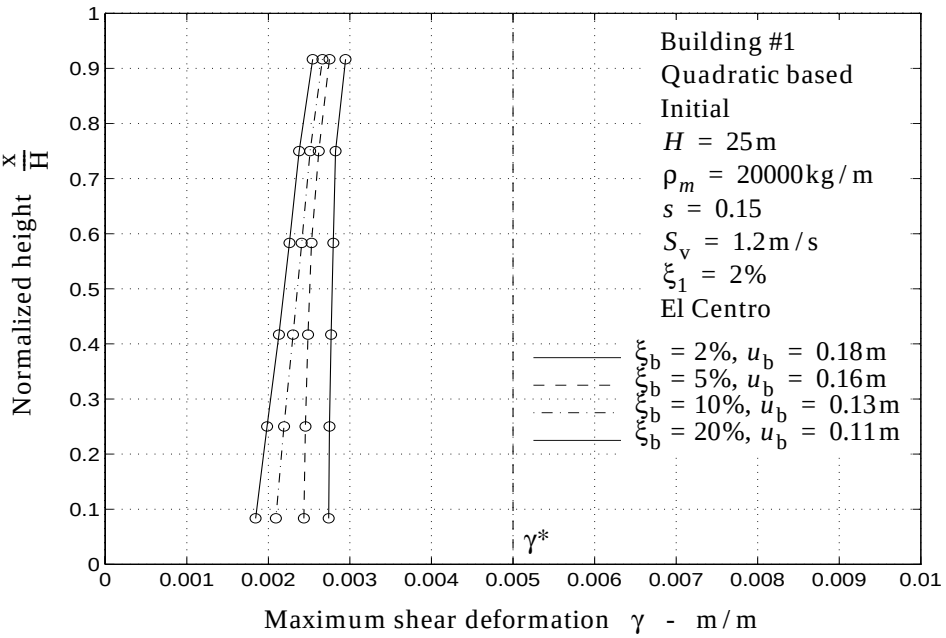

Fig. 5.41: Maximum shear deformation for Building 1.

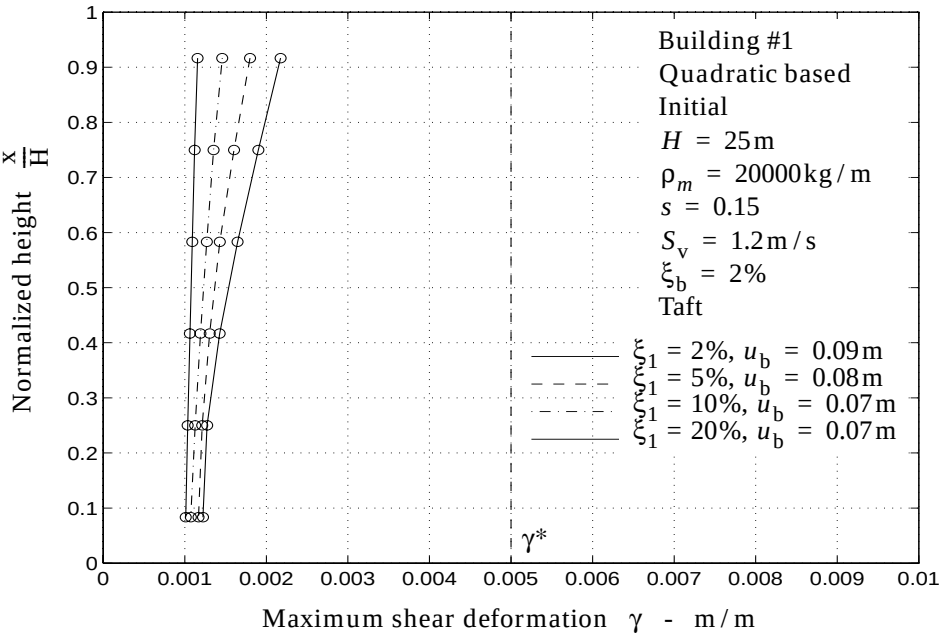

Fig. 5.42: Maximum shear deformation for Building 1.

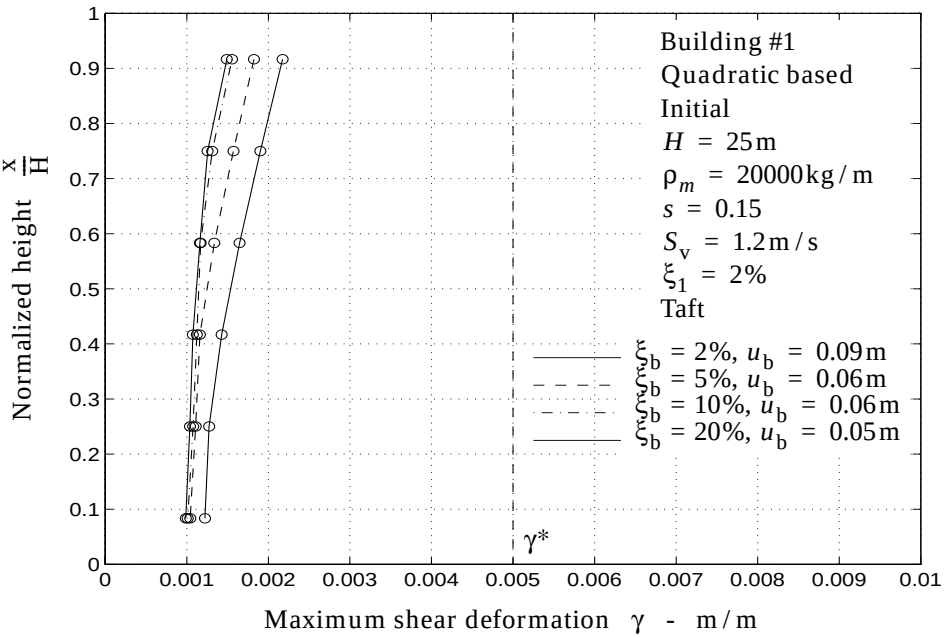

Fig. 5.43: Maximum shear deformation for Building 1.

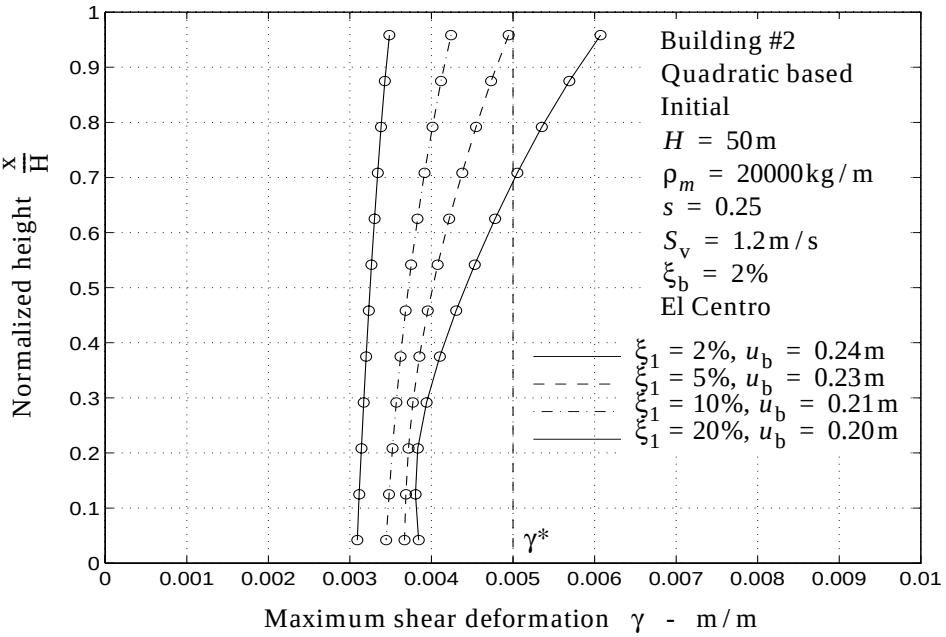

Fig. 5.44: Maximum shear deformation for Building 2.

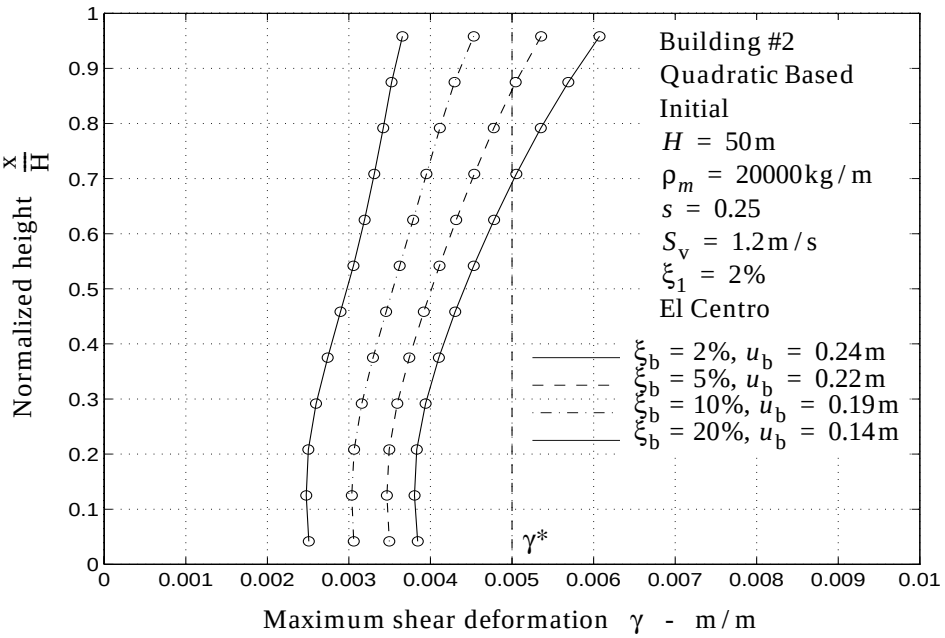

Fig. 5.45: Maximum shear deformation for Building 2.

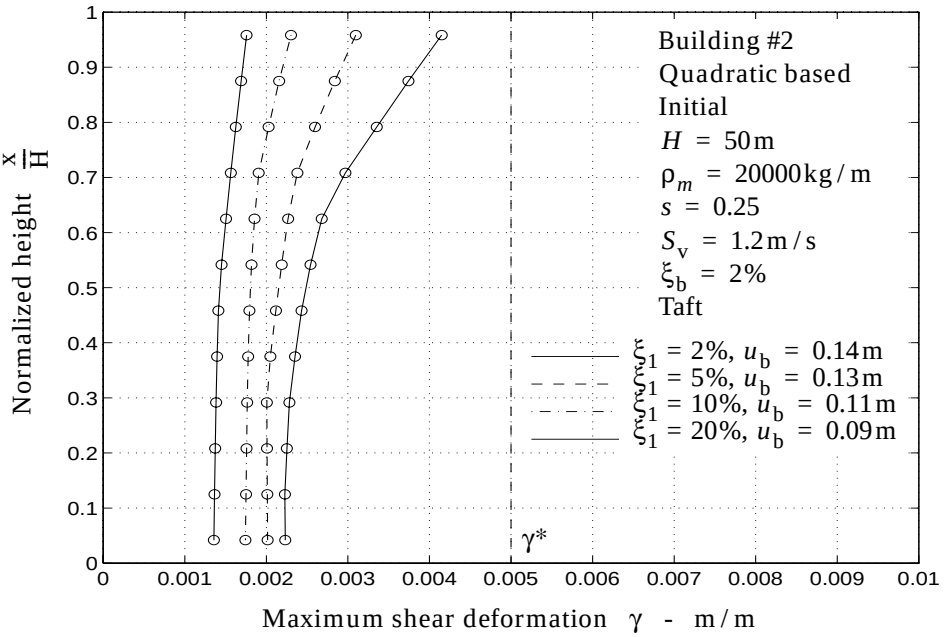

Fig. 5.46: Maximum shear deformation for Building 2.

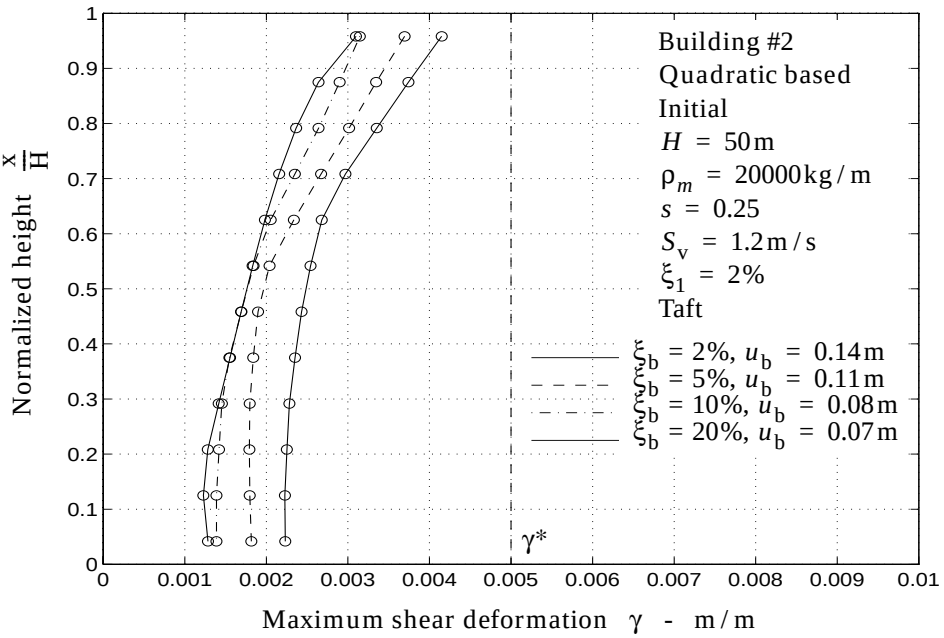

Fig. 5.47: Maximum shear deformation for Building 2.

Stiffness distribution including the contribution of the higher modes

This section extends the iterative procedure developed in Section 2.10 to incorporate iterating over the stiffness for the beam and isolator. For simplicity, only shear deformation in the isolator is considered. The method consists of including the contribution of the higher modes to the transverse shear, the bending deformation, and the base shear, and then updating the shear and bending rigidities and isolation stiffness using

$$D_{\mathrm{T}}^{(i+1)}(x) = D_{T}^{(i)} \frac{[\gamma^{(i)}(x)]_{\max}}{\gamma^{*}} \tag{5.134}$$

$$D_{\mathrm{B}}^{(i+1)}(x) = D_{B}^{(i)} \frac{[\chi^{(i)}(x)]_{\max}}{\chi^{*}} \tag{5.135}$$

$$k_{\mathrm{b}}^{(i+1)} = \frac{[V_{\mathrm{b}}^{(i)}]_{\max}}{u_{\mathrm{b}}{}^{*}} \tag{5.136}$$

The peak values are found with eqn (2.270).

Rigidity iterations are performed on building examples 1 and 2. Table 5.2 lists the parameters of the buildings for the initial rigidity distributions as well as for a single iteration. For both building examples, one iteration was sufficient to achieve convergence.Tables 5.3 and 5.4 contain the deformations averaged over the height of the structure and the corresponding standard deviations for Buildings 1 and 2 subjected to scaled versions of El Centro and Taft excitations.

Table 5.2: Modal parameters - building examples.

	T_1(s)	T_2(s)	T_3(s)	ξ_1(%)	ξ_2(%)	ξ_3(%)	Γ_2/Γ_1	Γ_3/Γ_1
Bldg #1								
Initial (Q)	2.09	0.62	0.33	1.56	3.55	6.26	0.11	0.03
Iteration 1	2.01	0.60	0.32	1.54	3.64	6.37	0.12	0.03
Bldg #2								
Initial (Q)	2.51	0.90	0.49	1.48	3.70	6.60	0.20	0.06
Iteration 1	2.45	0.85	0.46	1.48	3.83	6.89	0.19	0.06

Figures 5.48 through 5.57 show the shear and bending rigidity distributions resulting from the first iteration, as well as the shear deformation profiles corresponding to different combinations of building damping ratios and isolator damping ratios under El Centro and Taft excitation.Results from one iteration provide sufficient convergence accuracy. For Building 2, the iterative scheme tends to pull the top back in, resulting in a more uniform deformation profile. The effect of damping is similar to that noticed in the examples of the previous section.

Table 5.3: Mean and standard deviation deformation results for Building 1.

Bldg #1	ξ_1 (%)	ξ_b (%)	u_b (m)	γ_m (10^{-3})	γ_{sd} (10^{-4})	χ_m (10^{-5})	χ_{sd} (10^{-6})
El Centro							
Initial (Q)	2.00	2.00	0.18	2.80	0.70	3.18	0.56
	5.00	2.00	0.18	2.74	0.46	3.11	0.31
	10.00	2.00	0.17	2.61	0.11	2.93	0.07
	20.00	2.00	0.17	2.43	0.22	2.72	0.24
	2.00	2.00	0.18	2.80	0.70	3.18	0.56
	2.00	5.00	0.16	2.55	1.09	2.93	0.95
	2.00	10.00	0.13	2.36	1.92	2.79	1.31
	2.00	20.00	0.11	2.19	2.35	2.62	1.57
Iteration 1	2.00	2.00	0.17	3.28	1.36	2.86	4.40
	5.00	2.00	0.17	3.09	1.05	2.68	4.31
	10.00	2.00	0.15	2.79	0.66	2.41	4.10
	20.00	2.00	0.15	2.37	0.62	1.98	3.63
	2.00	2.00	0.17	3.28	1.36	2.86	4.40
	2.00	5.00	0.14	2.55	1.23	2.22	3.08
	2.00	10.00	0.12	2.26	0.92	1.96	3.21
	2.00	20.00	0.10	2.16	1.38	1.90	2.98
Taft							
Initial (Q)	2.00	2.00	0.09	1.61	3.42	2.04	2.76
	5.00	2.00	0.08	1.42	2.22	1.74	1.86
	10.00	2.00	0.07	1.25	1.32	1.49	0.96
	20.00	2.00	0.07	1.08	0.49	1.25	0.31
	2.00	2.00	0.09	1.61	3.42	2.04	2.76
	2.00	5.00	0.06	1.34	2.78	1.67	2.60
	2.00	10.00	0.06	1.21	1.80	1.45	1.79
	2.00	20.00	0.05	1.17	1.68	1.41	1.54
Iteration 1	2.00	2.00	0.08	1.80	2.26	1.64	2.00
	5.00	2.00	0.08	1.57	1.00	1.38	1.97
	10.00	2.00	0.08	1.38	0.39	1.19	1.97
	20.00	2.00	0.07	1.17	0.27	0.99	1.84
	2.00	2.00	0.08	1.80	2.26	1.64	2.00
	2.00	5.00	0.07	1.41	1.73	1.27	1.45
	2.00	10.00	0.06	1.25	0.63	1.07	1.43
	2.00	20.00	0.05	1.22	0.93	1.07	1.29

Table 5.4: Mean and standard deviation deformation results for Building 2.

Bldg #2	ξ_1 (%)	ξ_b (%)	u_b (m)	γ_m (10^{-3})	γ_{sd} (10^{-4})	χ_m (10^{-5})	χ_{sd} (10^{-6})
El Centro							
Initial (Q)	2.00	2.00	0.24	4.61	7.49	4.90	5.96
	5.00	2.00	0.23	4.13	4.17	4.25	3.28
	10.00	2.00	0.21	3.77	2.49	3.81	1.83
	20.00	2.00	0.20	3.26	1.22	3.25	0.81
	2.00	2.00	0.24	4.61	7.49	4.90	5.96
	2.00	5.00	0.22	4.15	6.25	4.39	4.88
	2.00	10.00	0.19	3.61	4.98	3.79	3.72
	2.00	20.00	0.14	2.99	4.10	3.15	2.78
Iteration 1	2.00	2.00	0.23	4.67	4.36	4.04	5.92
	5.00	2.00	0.22	4.11	1.84	3.44	5.67
	10.00	2.00	0.21	3.65	1.68	2.98	5.54
	20.00	2.00	0.20	3.12	2.34	2.50	5.14
	2.00	2.00	0.23	4.67	4.36	4.04	5.92
	2.00	5.00	0.21	4.21	3.61	3.62	5.43
	2.00	10.00	0.18	3.65	2.87	3.12	4.82
	2.00	20.00	0.14	2.98	2.43	2.55	4.15
Taft							
Initial (Q)	2.00	2.00	0.14	2.77	6.24	3.00	5.56
	5.00	2.00	0.13	2.30	3.49	2.41	3.19
	10.00	2.00	0.11	1.89	1.74	1.91	1.74
	20.00	2.00	0.09	1.49	1.33	1.52	1.17
	2.00	2.00	0.14	2.77	6.24	3.00	5.56
	2.00	5.00	0.11	2.34	6.53	2.56	6.05
	2.00	10.00	0.08	1.99	6.03	2.23	4.98
	2.00	20.00	0.07	1.87	5.69	2.16	4.48
Iteration 1	2.00	2.00	0.11	2.45	4.92	2.22	2.84
	5.00	2.00	0.10	2.05	2.68	1.80	2.38
	10.00	2.00	0.09	1.69	1.22	1.43	2.03
	20.00	2.00	0.08	1.38	0.75	1.16	2.00
	2.00	2.00	0.11	2.45	4.92	2.22	2.84
	2.00	5.00	0.09	2.16	4.57	1.97	2.73
	2.00	10.00	0.08	1.87	3.92	1.69	2.47
	2.00	20.00	0.07	1.74	2.93	1.57	1.72

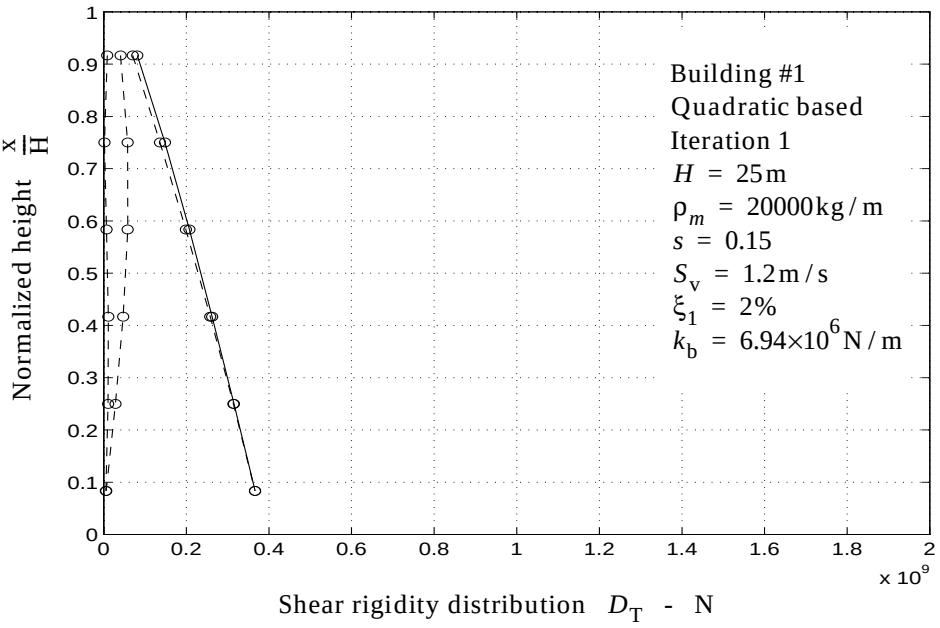

Fig. 5.48: Converged shear rigidity distribution for Building 1.

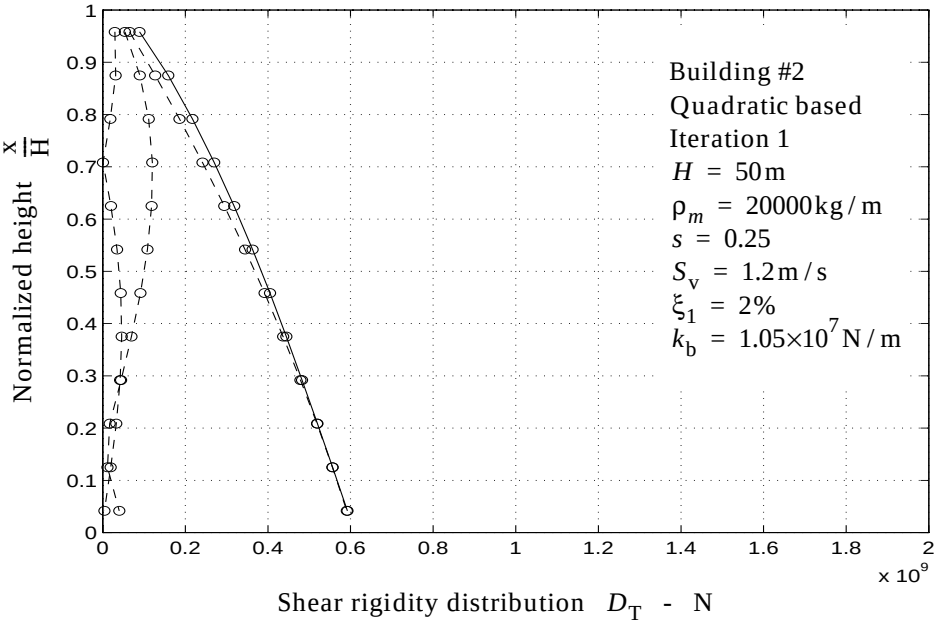

Fig. 5.49: Converged shear rigidity distribution for Building 2.

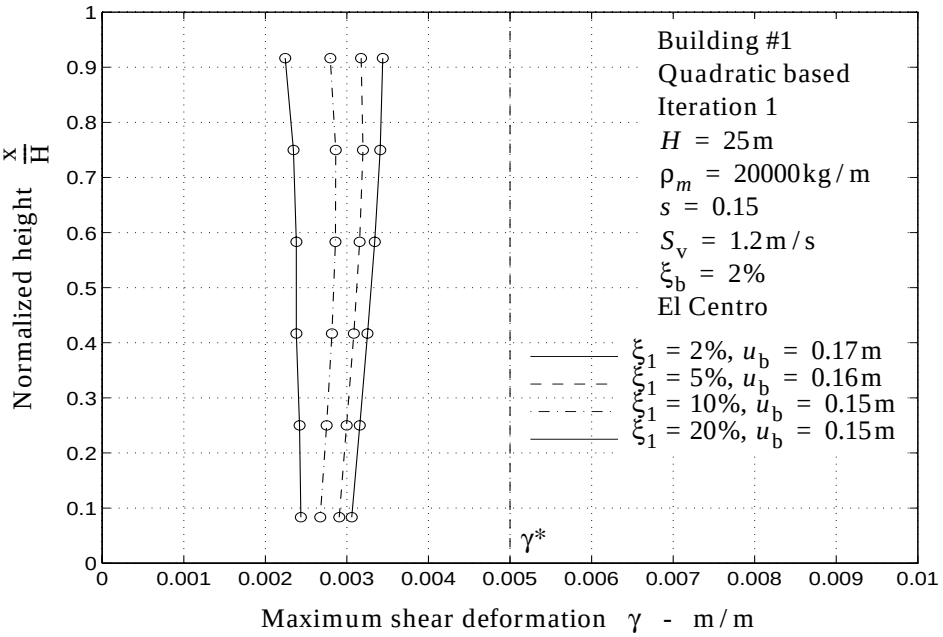

Fig. 5.50: Maximum shear deformation for Building 1.

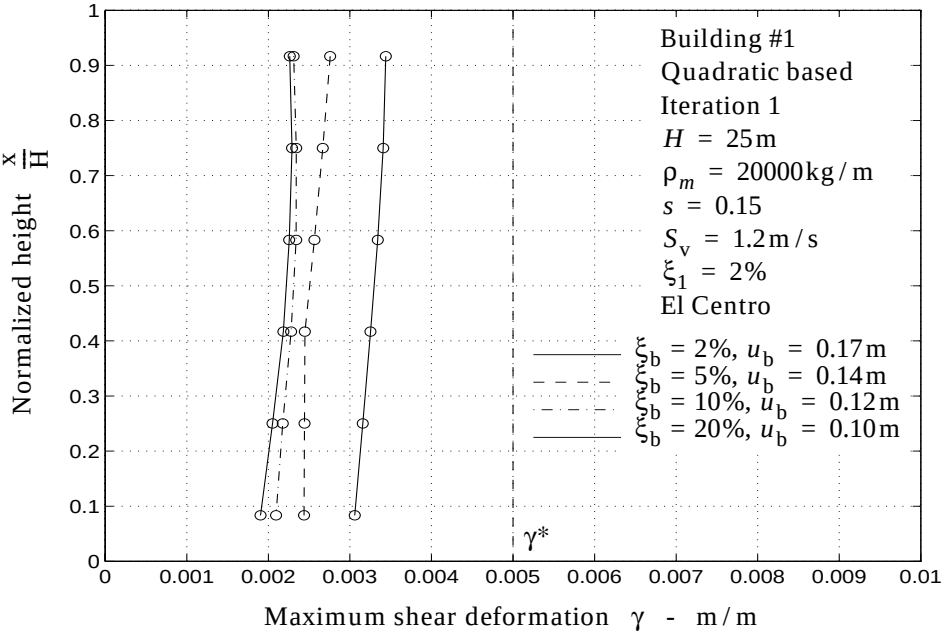

Fig. 5.51: Maximum shear deformation for Building 1.

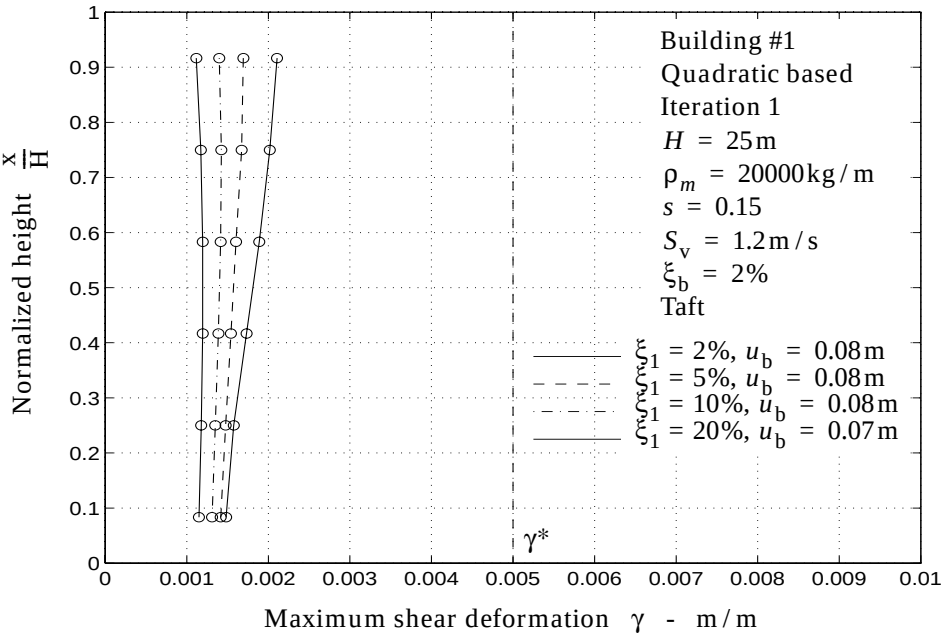

Fig. 5.52: Maximum shear deformation for Building 1.

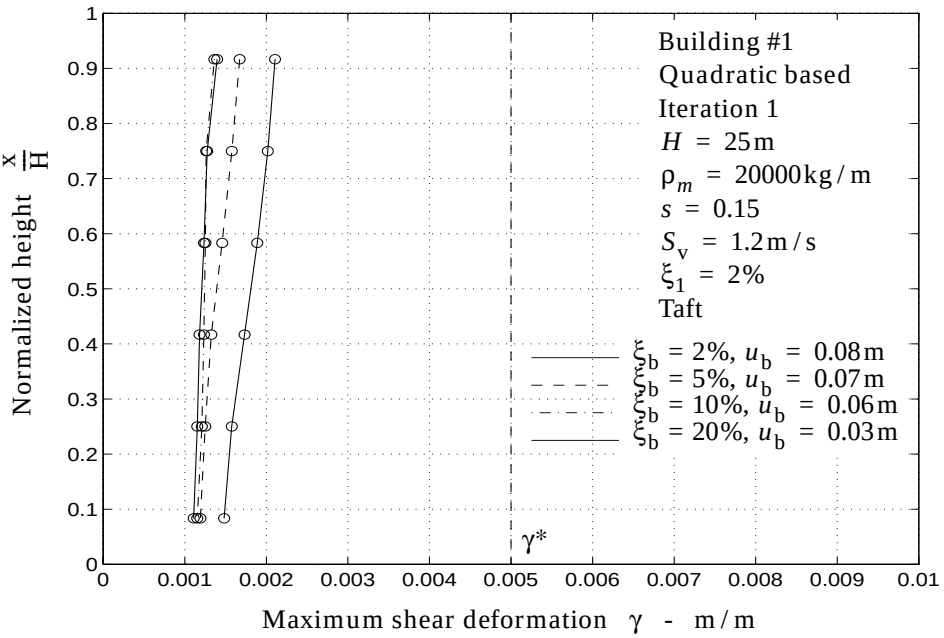

Fig. 5.53: Maximum shear deformation for Building 1.

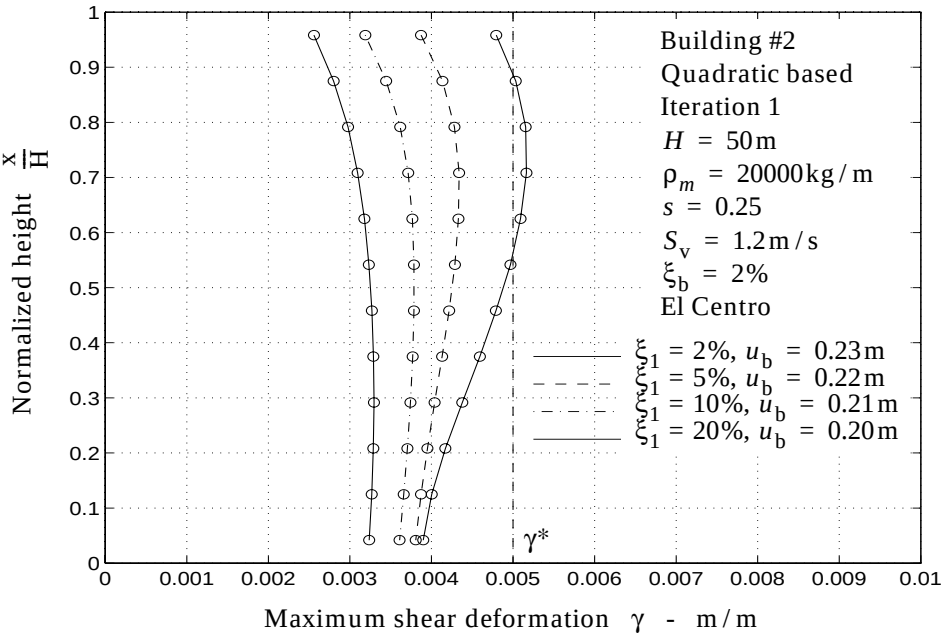

Fig. 5.54: Maximum shear deformation for Building 2.

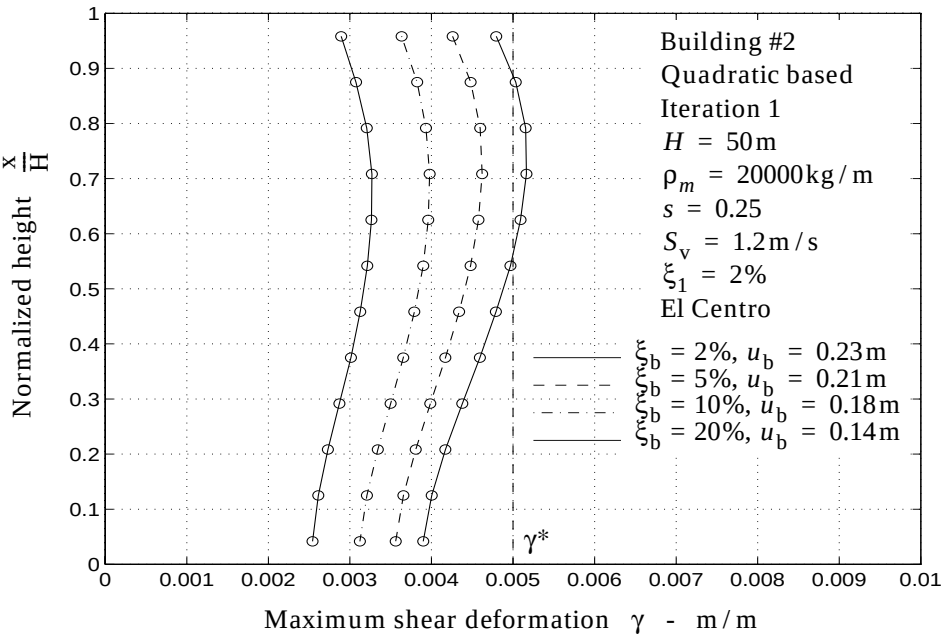

Fig. 5.55: Maximum shear deformation for Building 2.

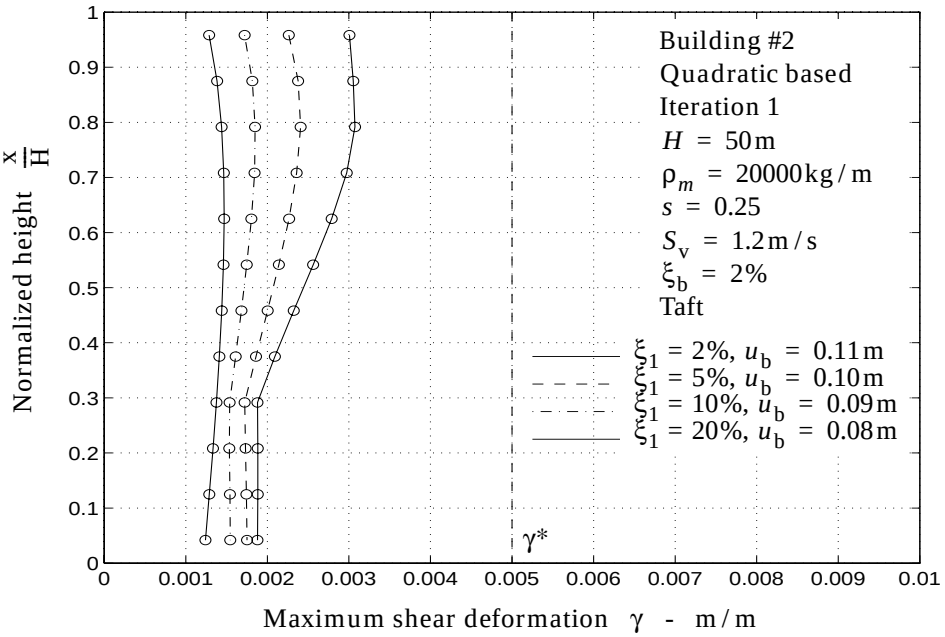

Fig. 5.56: Maximum shear deformation for Building 2.

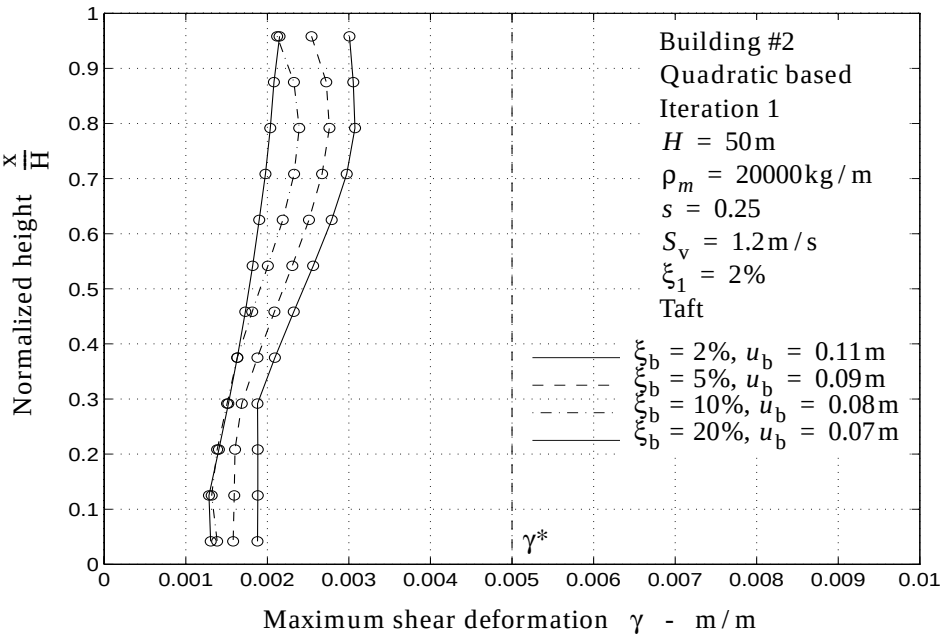

Fig. 5.57: Maximum shear deformation for Building 2.